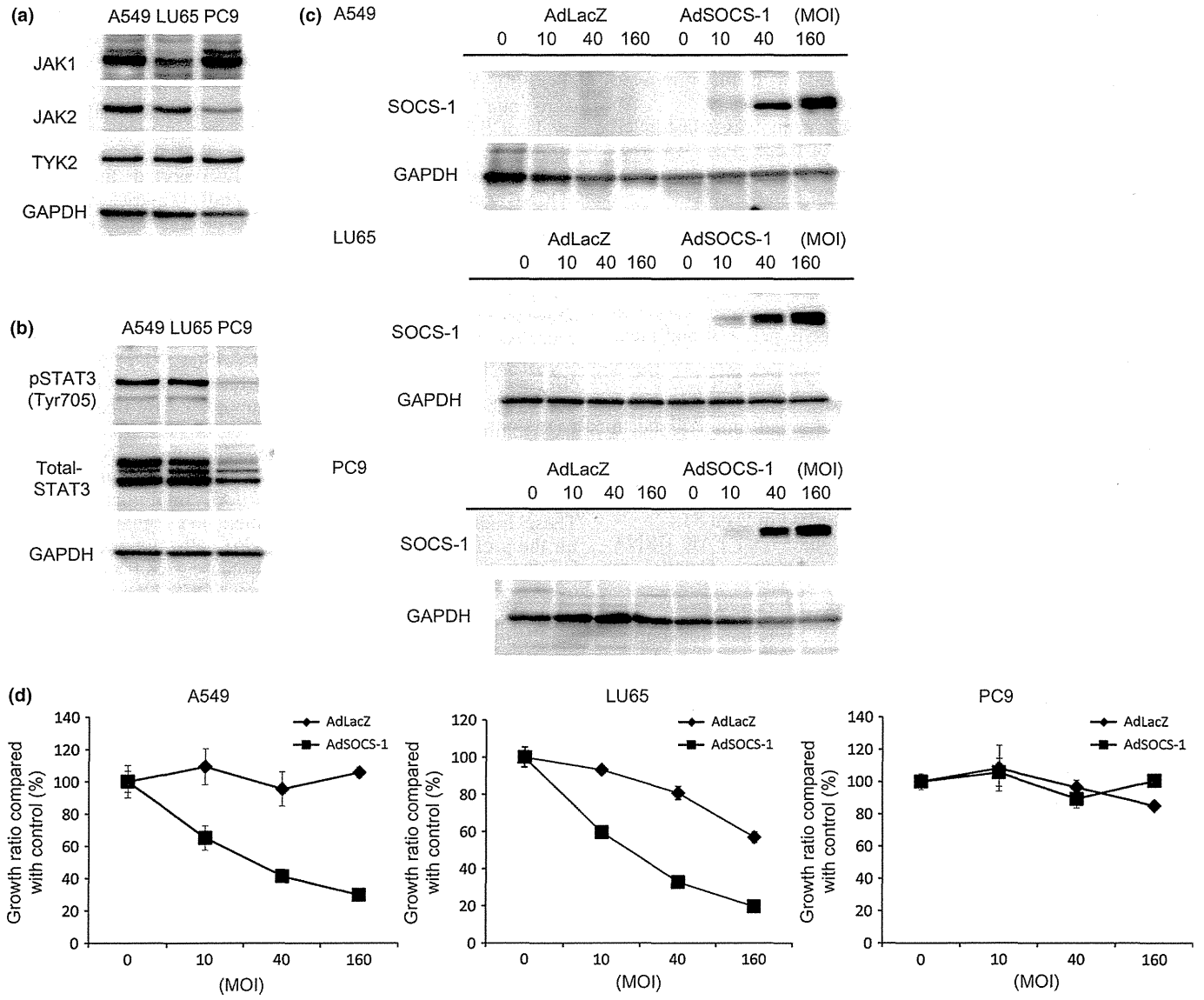


Fig. 1. Delivery of *SOCS-1* gene shows marked antiproliferative effects in A549 and LU65 lung cancer cell lines. (a) Expression of JAK family kinases in all cell lines determined by Western blotting. Cell lysates were immunoblotted with JAK1, JAK2, or tyrosine kinase 2 (TYK2) antibodies. (b) Comparative analysis of phosphorylation and expression of signal transducer and activator of transcription 3 (STAT3) determined by Western blotting. (c) Cell lysates were prepared 48 h after treatment with AdSOCS-1or AdLacZ adenoviral vectors at an MOI of 10–160, and immunoblotted with anti-SOCS-1 antibody. (d) Cells were infected with AdSOCS-1 or AdLacZ at an MOI of 10–160. Cell proliferation was determined by MTS assay 72 h after transfection. Growth ratio of AdLacZ or AdSOCS-1-infected cells was calculated by a percentage of that for non-treated cells. Each value represents the average ± SD of hexaplicate wells.

the combined effect of JAK inhibitor I and FAK siRNA on A549 cell proliferation. The results showed that the combined effect was stronger than that of JAK inhibitor I alone (Fig. 3e). These findings suggest that FAK has an important role in A549 cell proliferation independent of JAK and that SOCS-1-mediated FAK inhibition might contribute to the suppression of proliferation of A549 cells treated with AdSOCS-1.

Epidermal growth factor receptor is downregulated by overexpression of SOCS-1 in A549. Expression of SOCS-1 reportedly interacts with the cytoplasmic domain of EGFR and is likely to induce ubiquitination and degradation of ligand-bound EGFR.[33] This notion was confirmed by means of immunoblotting analysis in our study, in that EGFR expression was downregulated 48 h after introduction of the *SOCS-1* gene in A549 cells. The EGFR phosphorylation (Tyr1068) was also downregulated after overexpression of the *SOCS-1* gene had occurred in A549 cells (Fig. 4a). In contrast, JAK inhibitor I did not suppress EGFR activation in A549 cells (Fig. 4b).

We next examined the antiproliferative effects of the EGFR inhibitor PD153035 on A549 cells. Expression of EGFR in A549 cells was much lower than that in PC9 cells (data not shown), which harbor a deletion of an EGFR mutation.[34] Nevertheless, our findings show that proliferation of A549 cells with wild-type EGFR were also somewhat dependent on EGFR (Fig. 4c,d). We also investigated the combined effect of JAK inhibitor I and PD153035 on proliferation of A549 cells and found that they have an additive effect (Fig. 4e). This finding suggests that EGFR is also involved in A549 cell proliferation independent of JAK and that its downregulation by SOCS-1 may have an inhibitory effect on proliferation of A549 cells.

© 2013 Japanese Cancer Association

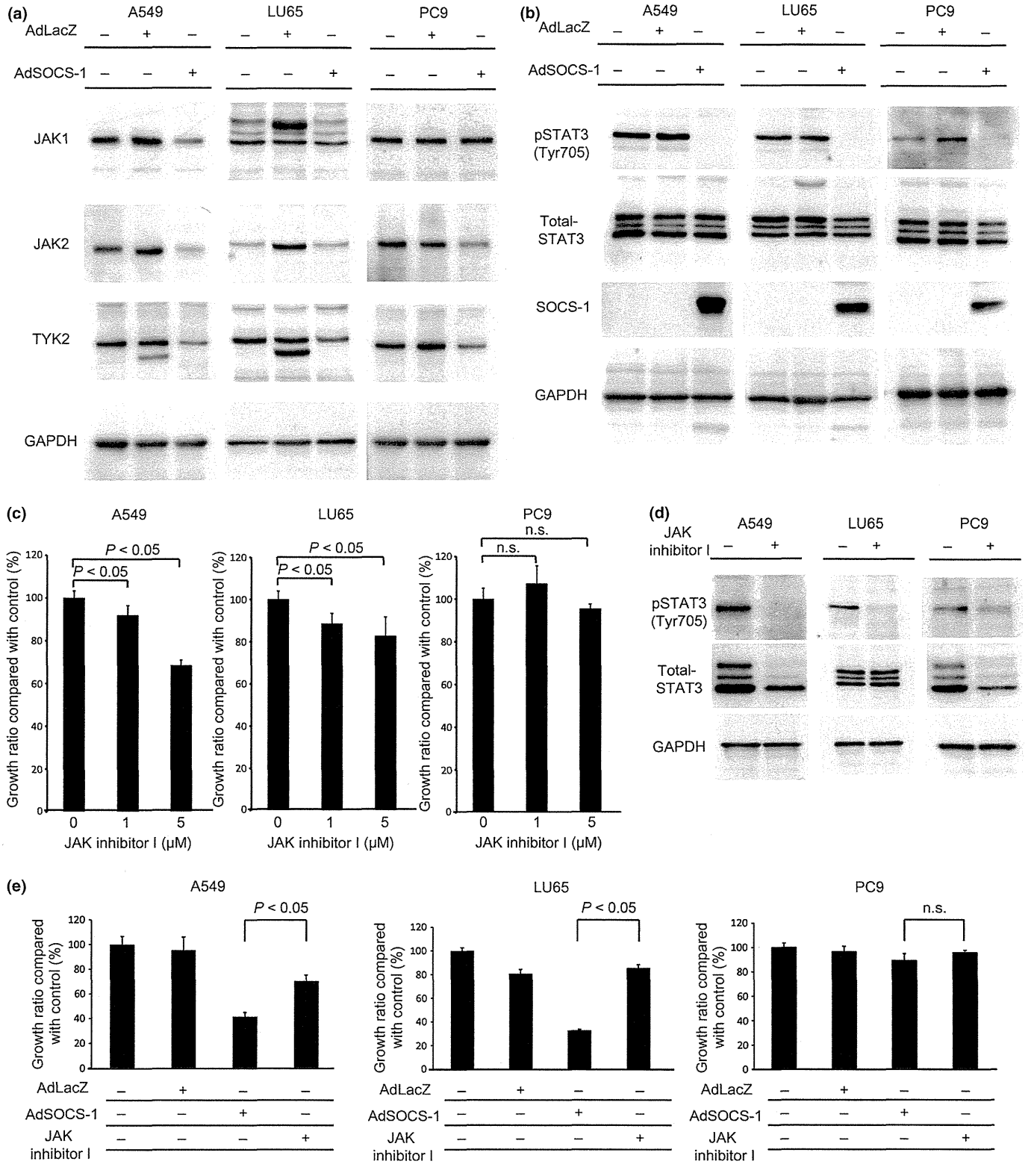


Fig. 2. Antiproliferative effect of suppressor of cytokine signaling-1 (SOCS-1) correlated with JAK dependence is stronger than JAK inhibitor. (a) Cell lysates were prepared 48 h after treatment with AdSOCS-1 or AdLacZ adenoviral vectors at an MOI of 40 and immunoblotted with JAK1, JAK2, or tyrosine kinase 2 (TYK2) antibodies. (b) SOCS-1 suppressed activation of signal transducer and activator of transcription 3 (STAT3). Cell lysates were prepared as described above and immunoblotted with anti-p-STAT3 (Tyr705), anti-STAT3, and anti-SOCS-1 antibodies. (c) Cells cultured in RPMI-1640 medium containing 10% FBS were exposed to 1–5 μM JAK inhibitor I. After incubation for 72 h, viable cells were counted with the MTS assay. (d) Cells were cultured in RPMI-1640 medium containing 0.5% FBS with 5 μM JAK inhibitor I. Cell lysates were immunoblotted with anti-p-STAT3 (Tyr705) and anti-STAT3 antibodies. (e) All cell lines cultured in RPMI-1640 medium containing 10% FBS were exposed to 5 μM JAK inhibitor I, or infected with AdLacZ or AdSOCS-1 at an MOI of 40. After incubation for 72 h, viable cells were counted with the MTS assay.

doi: 10.1111/cas.12266
© 2013 Japanese Cancer Association

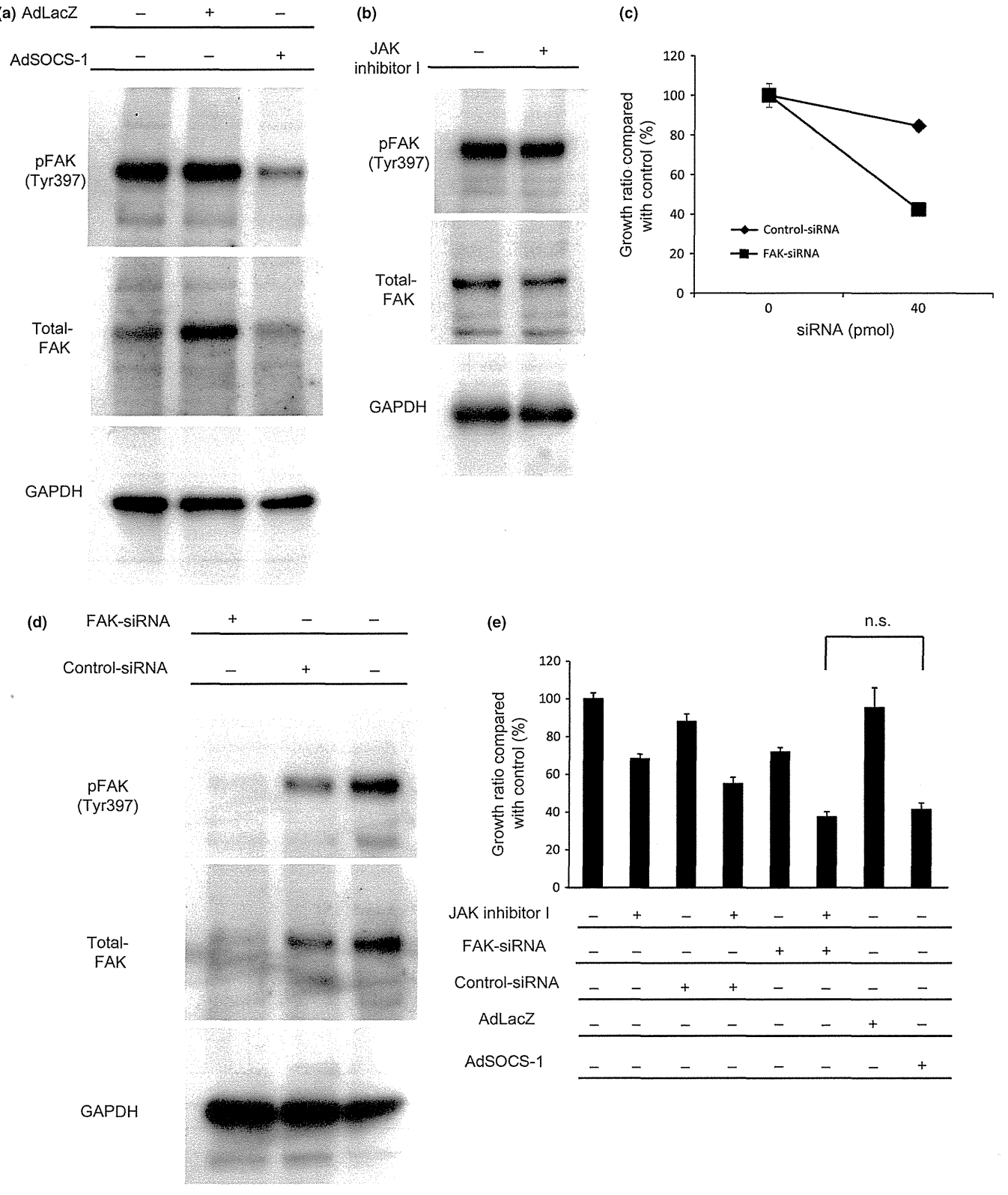


Fig. 3. Focal adhesion kinase (FAK) is downregulated by adenovirus vector containing suppressor of cytokine signaling-1 (AdSOCS-1) in A549 lung cancer cells. (a) Cell lysates were prepared 48 h after treatment with AdSOCS-1 or AdLacZ at an MOI of 40, and immunoblotted with p-FAK (Tyr397) and FAK antibodies. (b) Cell lysates were prepared 48 h after exposure to 5 μM JAK inhibitor I and immunoblotted with p-FAK (Tyr397) and FAK antibodies. (c) Cells were exposed to either FAK siRNA or non-specific siRNA as control. Cells were cultured in RPMI-1640 medium containing 10% FBS. After a 3-day culture, viable cells were counted with the MTS assay. (d) Protein extracts prepared at 48 h after treatment with FAK siRNA or non-specific siRNA were blotted with anti-p-FAK (Tyr397) and anti-FAK antibodies. (e) A549 cells cultured in RPMI-1640 medium containing 10% FBS were exposed to 5 μM JAK inhibitor I or 40 pmol FAK siRNA; 40 pmol non-specific siRNA was used as control. Infections of AdLacZ or AdSOCS-1 were carried out at an MOI of 40. Cell proliferation activity was assessed by MTS assay 72 h after treatment. n.s., no significant change detected by Tukey's post-hoc comparisons.

© 2013 Japanese Cancer Association

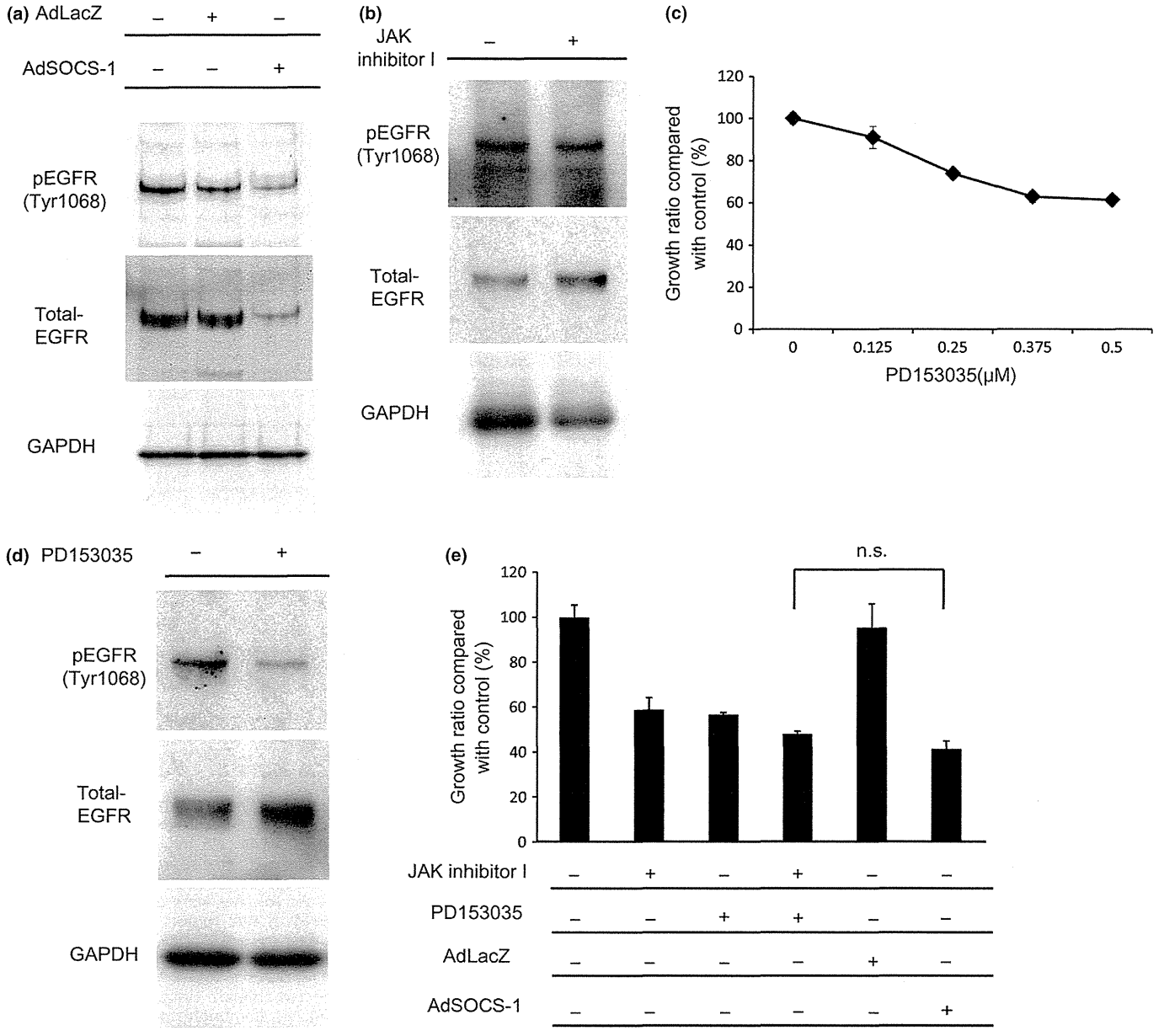


Fig. 4. Epidermal growth factor receptor (EGFR) is downregulated by adenovirus vector containing suppressor of cytokine signaling-1 (AdSOCS-1) in A549 lung cancer cells. (a) Cells were infected with AdLacZ or AdSOCS-1 at an MOI of 40 for 24 h. Cell lysates were immunoblotted with anti-p-EGFR (Tyr1068) and anti-EGFR antibodies. (b) Cell lysates were prepared 48 h after exposure to 5 μM JAK inhibitor I and immunoblotted with anti-p-EGFR (Tyr1068) and anti-EGFR antibodies. (c) Cells cultured in RPMI-1640 medium containing 10% FBS were exposed to 0.125–0.5 μM PD153035. Cell proliferation activity was assessed by MTS assay 72 h after exposure. (d) A549 cells were cultured in RPMI-1640 medium containing 0.5% FBS with 0.5 μM PD153035. Cell lysates were prepared 48 h after treatment and immunoblotted with anti-p-EGFR (Tyr1068) and anti-EGFR antibodies. (e) A549 cells cultured in RPMI-1640 medium containing 10% FBS were exposed to 5 μM JAK inhibitor I or 0.5 μM PD153035. Infection of AdLacZ or AdSOCS-1 was carried out at an MOI of 40. Cell proliferation activity was assessed by MTS assay 72 h after treatment. n.s., no significant change detected by Tukey's post-hoc comparisons.

Accordingly, JAK1, JAK2, FAK, and EGFR should be considered critical for the proliferation of A549 cells, so that simultaneous inhibition of these molecules by SOCS-1 may have a potent antiproliferative effect on A549.

Upregulation of p53 by AdSOCS-1 in A549 cells. We also used a phospho-kinase array to determine the expression profile of phosphorylated proteins in A549 in order to identify other target molecules for SOCS-1 in addition to JAK, FAK, and EGFR (Fig. 5a). Phosphorylation of p53 was upregulated in A549 cells after the introduction of the *SOCS-1* gene. This was confirmed by immunoblotting analysis, which showed that p53 phosphorylation was upregulated in A549 cells by overexpression of the *SOCS-1* gene (Fig. 5b). We also investigated whether JAK inhibitor I, instead of SOCS-1, could activate p53 in A549 cells, but found that it did not (Fig. 5b). Given the well-established antitumor effect of p53 phoshorylation,[35–38] SOCS-1-induced p53 activation may thus also contribute to the suppression of A549 cell proliferation.

Antitumor activity of *SOCS-1* in a lung cancer xenograft model. We also evaluated the therapeutic effect of AdSOCS-1 injection on the growth of NSCLC cells *in vivo*. We established a xenograft model of ICR nu/nu mice in which A549 cells were s.c. implanted. Injection of AdSOCS-1 vector

doi: 10.1111/cas.12266
© 2013 Japanese Cancer Association

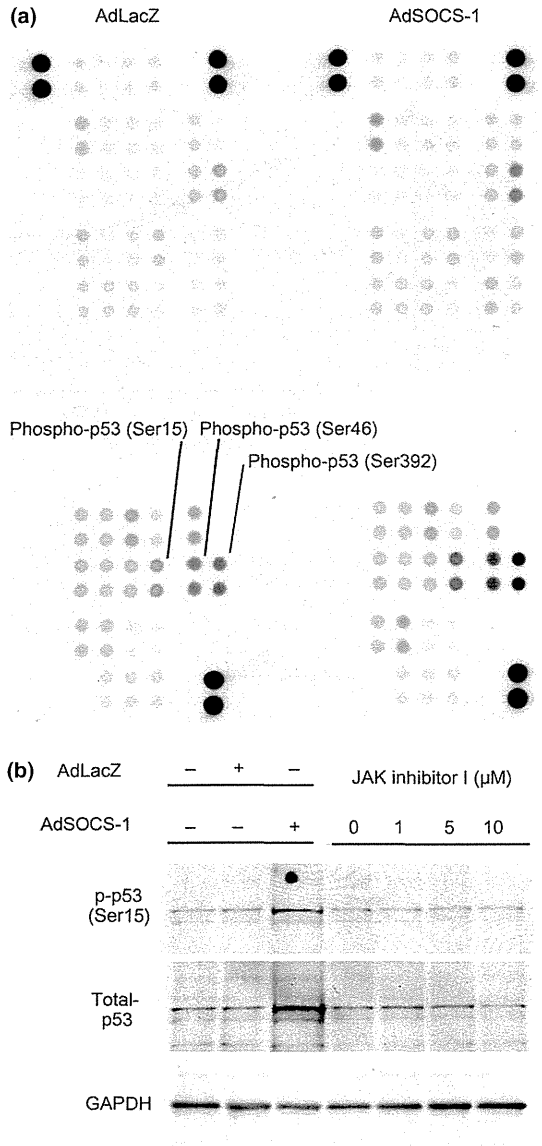


Fig. 5. Protein p53 is upregulated by adenovirus vector containing suppressor of cytokine signaling-1 (AdSOCS-1) in A549 lung cancer cells. (a) A549 cells were cultured in RPMI-1640 medium containing 10% FBS with AdSOCS-1 at an MOI of 40. After a 24-h culture, protein extracts were examined with a phospho-kinase array with each phosphorylated protein identified in duplicate. The double-labeled spots in the upper right corner represent the positive controls. (b) Cell lysates were prepared 48 h after infection with AdLacZ or AdSOCS-1 at an MOI of 40. Cell lysates were immunoblotted with anti-phospho-53 (p-p53 [Ser15]) and anti-p53 antibodies. (c) Cell lysates were prepared 48 h after exposure to 5 μM JAK inhibitor I and immunoblotted with anti-p-p53 (Ser15) and anti-p53 antibodies.

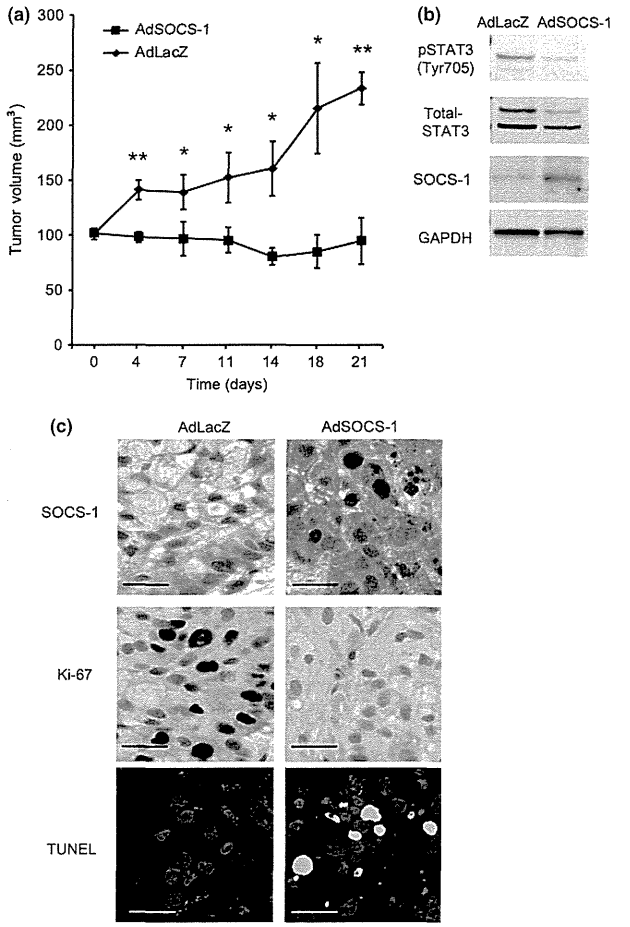


Fig. 6. Suppressor of cytokine signaling-1 (SOCS-1) shows antitumor activity in a lung cancer xenograft model. (a) Female ICR nu/nu mice were s.c. implanted with 2×10^6 A549 cells in their flank. When the calculated tumor volumes reached to approximately 100 mm^3, 4×10^8 pfu AdSOCS1 or AdLacZ adenoviral vectors were intratumorally treated twice per week. Tumor volumes were determined twice per week. The mean volume ± SEM of five tumors in each group, and were analyzed by Student's *t*-test (*$P < 0.05$, **$P < 0.01$). (b) Western blot analysis of phosphorylated signal transducer and activator of transcription 3 (pSTAT3), STAT3, SOCS-1, and GAPDH in A549 tissues from AdSOCS-1 or AdLacZ injected animals. Lysates from tumors were analyzed by Western blotting. (c) Immunohistochemical analysis of SOCS-1, Ki-67, and TUNEL (blue fluorescence, DAPI staining for nuclei; cyan fluorescence, TUNEL positivity) in A549 tissues from animals injected with AdSOCS-1 or AdLacZ. Scale bar = 25 μm.

(4×10^8 pfu) intratumorally twice per week significantly suppressed tumor growth compared to control AdLacZ injection (Fig. 6a). AdSOCS-1 *in vivo* could modulate intracellular signaling in NSCLC cells as *in vitro*, as Western blot analysis showed that phosphorylation levels of STAT3 were decreased in the A549 tissues from AdSOCS-1 injected animals (Fig. 6b). Furthermore, few Ki-67-positive nuclei were detected by immunohistochemical analysis in AdSOCS-1 infected tissues compared to AdLacZ, indicating that proliferating cells are decreased by overexpression of SOCS-1 (Fig. 6c). Additionally, induction of apoptosis was detected in AdSOCS-1 infected A549 tissue compared to AdLacZ by TUNEL analysis (Fig. 6c).

Discussion

In this study, we investigated the possibility that SOCS-1 could be used in LC therapies. Previous reports showed that PC9 harbors a deletion mutation in EGFR and that A549 and LU65 cells possess wild-type EGFR.[34,39] Although EGFR mutation in NSCLC was previously reported to activate AKT, MAPK, and STAT3 signaling,[40] our research showed that STAT3 was more strongly expressed in A549 and LU65 than in PC9 cells, and that sensitivity to overexpression of SOCS-1 was also higher in A549 and LU65 cells than in PC9 (Fig. 1). In addition, JAK inhibitor I significantly suppressed proliferation of A549 and LU65 cells, but not of PC9. Therefore, we consider that the marked antiproliferative effect by overexpression of SOCS-1 on A549 and LU65 cells, but not on PC9, was

© 2013 Japanese Cancer Association

attributable to the inhibition of JAK/STAT3 pathway *in vitro*. As SOCS-1 also shows an antiproliferative effect *in vivo* (Fig. 6), AdSOCS1 gene therapy might be effective for patients with NSCLC, in which the JAK/STAT3 signaling pathway is constitutively activated. It has been reported that approximately 50% of NSCLC tumors showed elevated phosphorylation levels of STAT3 (Tyr705) by immunohistochemical analysis.[4] There is a further possibility that LC patients harboring STAT3 dependence, detected by immunostaining analysis of phosphorylation levels of STAT3 (Tyr705) in specimens obtained surgically or bronchoscopically, could be selected for treatment with SOCS-1 overexpression.

Comparative analyses of the antiproliferative effects of *SOCS-1* gene introduction and JAK inhibitor I treatment suggest that overexpression of SOCS-1 may have a stronger effect than that of the JAK inhibitor I on A549 and LU65 cells (Fig. 2e). In fact, SOCS-1, but not JAK inhibitor I, inhibited FAK and EGFR, which are important for the survival of A549 cells. In addition, the combined effect of FAK siRNA and JAK inhibitor I, or that of PD153035 and JAK inhibitor I, was superior to the antiproliferative effect of JAK inhibitor alone (Figs 3,4). These findings suggest that the potent antiproliferative effect of SOCS-1 depends not only on JAK inhibition but also on the suppression of other distinct signal transduction pathways, such as FAK and EGFR. In addition, phosphorylation of p53 at Ser15 was enhanced by the overexpression of the *SOCS-1* gene in A549 cells (Fig. 5). Because phosphorylation of p53 at Ser15 contributes to antitumor effects under certain experimental conditions,[35–38] and A549 cells express wild-type p53,[41] activation of p53 by SOCS-1 overexpression seems to be involved in the antitumor effects.[42]

In conclusion, the findings of our study suggest that *SOCS-1* gene therapy is potentially effective for at least a subset of NSCLC both *in vitro* and *in vivo*. It was shown that SOCS-1 had a potent antiproliferative effect on JAK-dependent NSCLC cells by targeting the JAK/STAT3 pathway. In addition, SOCS-1 successfully targeted many factors such as FAK, EGFR, and p53 in NSCLC cells. It is thus possible that *SOCS-1* gene therapy could have a unique advantage over JAK inhibitor for the treatment of NSCLC.

Further studies will be needed to elucidate the mechanism of JAK/STAT3 pathway-dependence in NSCLC, and to validate the benefits that *SOCS-1* gene therapy could provide for NSCLC treatment in clinical practice.

Acknowledgments

This work was supported by a Grant-in-Aid from the Ministry of Health, Labour and Welfare, Japan (T. Naka) and a grant from the Kansai Biomedical Cluster Project in Saito, which is promoted by the Knowledge Cluster Initiative of the Ministry of Education, Culture, Sports, Science and Technology, Japan (T. Naka). The authors are grateful to Ms. M. Urase for experimental assistance and Ms. Y. Kanazawa and Ms. J. Yamagishi for secretarial assistance.

Disclosure Statement

The authors have no conflict of interest.

Abbreviations

AdSOCS-1	adenovirus vector containing SOCS-1
EGFR	epidermal growth factor receptor
FAK	focal adhesion kinase
LC	lung cancer
NSCLC	non-small-cell lung cancer
SOCS	suppressor of cytokine signaling
STAT	signal transducer and activator of transcription
TYK	tyrosine kinase

References

1 Hattori M, Fujita M, Ito Y, Ioka A, Katanoda K, Nakamura Y. Use of a population-based cancer registry to calculate twenty-year trends in cancer incidence and mortality in Fukui Prefecture. *J Epidemiol* 2010; **20**: 244–52.
2 Goffin J, Lacchetti C, Ellis PM, Ung YC, Evans WK. First-line systemic chemotherapy in the treatment of advanced non-small cell lung cancer: a systematic review. *J Thorac Oncol* 2010; **5**: 260–74.
3 Rossi A, Di Maio M, Chiodini P *et al.* Carboplatin- or cisplatin-based chemotherapy in first-line treatment of small-cell lung cancer: the COCIS meta-analysis of individual patient data. *J Clin Oncol* 2012; **30**: 1692–8.
4 Gao SP, Mark KG, Leslie K *et al.* Mutations in the EGFR kinase domain mediate STAT3 activation via IL-6 production in human lung adenocarcinomas. *J Clin Invest* 2007; **117**: 3846–56.
5 Lai SY, Johnson FM. Defining the role of the JAK-STAT pathway in head and neck and thoracic malignancies: implications for future therapeutic approaches. *Drug Resist Updat* 2010; **13**: 67–78.
6 Song L, Rawal B, Nemeth JA, Haura EB. JAK1 activates STAT3 activity in non-small-cell lung cancer cells and IL-6 neutralizing antibodies can suppress JAK1-STAT3 signaling. *Mol Cancer Ther* 2011; **10**: 481–94.
7 Guo Y, Xu F, Lu T, Duan Z, Zhang Z. Interleukin-6 signaling pathway in targeted therapy for cancer. *Cancer Treat Rev* 2012; **38**: 904–10.
8 Jiang R, Jin Z, Liu Z, Sun L, Wang L, Li K. Correlation of activated STAT3 expression with clinicopathologic features in lung adenocarcinoma and squamous cell carcinoma. *Mol Diagn Ther* 2011; **15**: 347–52.
9 Verstovsek S, Kantarjian H, Mesa RA *et al.* Safety and efficacy of INCB018424, a JAK1 and JAK2 inhibitor, in myelofibrosis. *N Engl J Med* 2010; **363**: 1117–27.
10 Naka T, Narazaki M, Hirata M *et al.* Structure and function of a new STAT-induced STAT inhibitor. *Nature* 1997; **387**: 924–9.
11 Starr R, Willson TA, Viney EM *et al.* A family of cytokine-inducible inhibitors of signalling. *Nature* 1997; **387**: 917–21.
12 Endo TA, Masuhara M, Yokouchi M *et al.* A new protein containing an SH2 domain that inhibits JAK kinases. *Nature* 1997; **387**: 921–4.
13 Piessevaux J, Lavens D, Peelman F, Tavernier J. The many faces of the SOCS box. *Cytokine Growth Factor Rev* 2008; **19**: 371–81.
14 Yoshimura A, Suzuki M, Sakaguchi R, Hanada T, Yasukawa H. SOCS, Inflammation, and Autoimmunity. *Front Immunol* 2012; **3**: 20.
15 Narazaki M, Fujimoto M, Matsumoto T *et al.* Three distinct domains of SSI-1/SOCS-1/JAB protein are required for its suppression of interleukin 6 signaling. *Proc Natl Acad Sci USA* 1998; **95**: 13130–4.
16 Yasukawa H, Misawa H, Sakamoto H *et al.* The JAK-binding protein JAB inhibits Janus tyrosine kinase activity through binding in the activation loop. *EMBO J* 1999; **18**: 1309–20.
17 Valentino L, Pierre J. JAK/STAT signal transduction: regulators and implication in hematological malignancies. *Biochem Pharmacol* 2006; **71**: 713–21.
18 Naka T, Fujimoto M, Tsutsui H, Yoshimura A. Negative regulation of cytokine and TLR signalings by SOCS and others. *Adv Immunol* 2005; **87**: 61–122.
19 Yoshimura A, Naka T, Kubo M. SOCS proteins, cytokine signalling and immune regulation. *Nat Rev Immunol* 2007; **7**: 454–65.
20 Zhang J, Li H, Yu JP, Wang SE, Ren XB. Role of SOCS1 in tumor progression and therapeutic application. *Int J Cancer* 2012; **130**: 1971–80.
21 Iwahori K, Serada S, Fujimoto M *et al.* Overexpression of SOCS3 exhibits preclinical antitumor activity against malignant pleural mesothelioma. *Int J Cancer* 2011; **129**: 1005–17.
22 Souma Y, Nishida T, Serada S *et al.* Antiproliferative effect of SOCS-1 through the suppression of STAT3 and p38 MAPK activation in gastric cancer cells. *Int J Cancer* 2012; **131**: 1287–96.
23 Iwahori K, Serada S, Fujimoto M *et al.* SOCS-1 gene delivery cooperates with cisplatin plus pemetrexed to exhibit preclinical antitumor activity against malignant pleural mesothelioma. *Int J Cancer* 2013; **132**: 459–71.
24 Baltayiannis G, Baltayiannis N, Tsianos EV. Suppressors of cytokine signaling as tumor repressors. Silencing of SOCS3 facilitates tumor formation and growth in lung and liver. *J BUON* 2008; **13**: 263–5.
25 Zhang S, Guo D, Jiang L, Zhang Q, Qiu X, Wang E. SOCS3 inhibiting migration of A549 cells correlates with PYK2 signaling in vitro. *BMC Cancer* 2008; **8**: 150.

doi: 10.1111/cas.12266
© 2013 Japanese Cancer Association

26 Lin YC, Lin CK, Tsai YH *et al.* Adenovirus-mediated SOCS3 gene transfer inhibits the growth and enhances the radiosensitivity of human non-small cell lung cancer cells. *Oncol Rep* 2010; **24**: 1605–12.
27 Mizuguchi H, Kay MA. A simple method for constructing E1- and E1/E4-deleted recombinant adenoviral vectors. *Hum Gene Ther* 1999; **10**: 2013–7.
28 Sakurai H, Tashiro K, Kawabata K *et al.* Adenoviral expression of suppressor of cytokine signaling-1 reduces adenovirus vector-induced innate immune responses. *J Immunol* 2008; **180**: 4931–8.
29 Verma A, Kambhampati S, Parmar S, Platanias LC. Jak family of kinases in cancer. *Cancer Metastasis Rev* 2003; **22**: 423–34.
30 Schmidmaier R, Baumann P. ANTI-ADHESION evolves to a promising therapeutic concept in oncology. *Curr Med Chem* 2008; **15**: 978–90.
31 Liu E, Cote JF, Vuori K. Negative regulation of FAK signaling by SOCS proteins. *EMBO J* 2003; **22**: 5036–46.
32 Kornberg LJ, Grant MB. Adenoviruses increase endothelial cell proliferation, migration, and tube formation: partial reversal by the focal adhesion kinase inhibitor, FRNK. *Microvasc Res* 2007; **73**: 157–62.
33 Quesnelle KM, Boehm AL, Grandis JR. STAT-mediated EGFR signaling in cancer. *J Cell Biochem* 2007; **102**: 311–9.
34 Zhang D, Takigawa N, Ochi N *et al.* Detection of the EGFR mutation in exhaled breath condensate from a heavy smoker with squamous cell carcinoma of the lung. *Lung Cancer* 2011; **73**: 379–80.
35 Lai JM, Chang JT, Wen CL, Hsu SL. Emodin induces a reactive oxygen species-dependent and ATM-p53-Bax mediated cytotoxicity in lung cancer cells. *Eur J Pharmacol* 2009; **623**: 1–9.
36 Amin AR, Wang D, Zhang H *et al.* Enhanced anti-tumor activity by the combination of the natural compounds (-)-epigallocatechin-3-gallate and luteolin: potential role of p53. *J Biol Chem* 2010; **285**: 34557–65.
37 Oh HL, Lee DK, Lim H, Lee CH. HY253, a novel decahydrofluorene analog, from Aralia continentalis, induces cell cycle arrest at the G1 phase and cytochrome c-mediated apoptosis in human lung cancer A549 cells. *J Ethnopharmacol* 2010; **129**: 135–9.
38 Yamada C, Ozaki T, Ando K *et al.* RUNX3 modulates DNA damage-mediated phosphorylation of tumor suppressor p53 at Ser-15 and acts as a co-activator for p53. *J Biol Chem* 2010; **285**: 16693–703.
39 Nagai Y, Miyazawa H, Huqun *et al.* Genetic heterogeneity of the epidermal growth factor receptor in non-small cell lung cancer cell lines revealed by a rapid and sensitive detection system, the peptide nucleic acid-locked nucleic acid PCR clamp. *Cancer Res* 2005; **65**: 7276–82.
40 Zimmer S, Kahl P, Buhl TM *et al.* Epidermal growth factor receptor mutations in non-small cell lung cancer influence downstream Akt, MAPK and Stat3 signaling. *J Cancer Res Clin Oncol* 2009; **135**: 723–30.
41 Kashii T, Mizushima Y, Monno S, Nakagawa K, Kobayashi M. Gene analysis of K-, H-ras, p53, and retinoblastoma susceptibility genes in human lung cancer cell lines by the polymerase chain reaction/single-strand conformation polymorphism method. *J Cancer Res Clin Oncol* 1994; **120**: 143–8.
42 Mallette FA, Calabrese V, Ilangumaran S, Ferbeyre G. SOCS1, a novel interaction partner of p53 controlling oncogene-induced senescence. *Aging (Albany NY)* 2010; **2**: 445–52.

Supporting Information

Additional supporting information may be found in the online version of this article:

Data S1. Methods.

© 2013 Japanese Cancer Association

JVI
Journals.ASM.org

Varicella-Zoster Virus ORF49 Functions in the Efficient Production of Progeny Virus through Its Interaction with Essential Tegument Protein ORF44

Tomohiko Sadaoka,[a,b] Satoshi Serada,[c] Junko Kato,[a] Mayuko Hayashi,[a,b] Yasuyuki Gomi,[d] Tetsuji Naka,[c] Koichi Yamanishi,[e] Yasuko Mori[a,b]

Division of Clinical Virology, Center for Infectious Diseases, Kobe University Graduate School of Medicine, Kusunoki-cho, Chuo-ku, Kobe, Japan[a]; Laboratory of Virology and Vaccinology, Division of Biomedical Research, National Institute of Biomedical Innovation, Saito-Asagi, Ibaraki, Osaka, Japan[b]; Laboratory of Immune Signal, Division of Biomedical Research, National Institute of Biomedical Innovation, Saito-Asagi, Ibaraki, Osaka, Japan[c]; Kanonji Institute, The Research Foundation for Microbial Diseases of Osaka University, Kanonji, Kagawa, Japan[d]; National Institute of Biomedical Innovation, Saito-Asagi, Ibaraki, Osaka, Japan[e]

The ORF49 tegument protein of varicella-zoster virus (VZV) is one of the core gene products that is conserved among herpesvirus family members. Although ORF49 is known to be a cell-tropic factor, its detailed functions remain elusive. ORF44 is another core gene product reported to be essential, although its characterization and detailed functional analysis have not been reported. These two core gene products form a complex in other herpesviruses beyond the host species and herpesvirus subfamilies. Here, we show that complex formation between ORF44 and ORF49 is conserved in VZV. We serendipitously found that binding is eliminated by an amino acid substitution at position 129 (phenylalanine 129), and four amino acids in the carboxyl-terminal half of the acidic cluster in ORF49 (i.e., aspartate-phenylalanine-aspartate-glutamate from positions 41 to 44 [41DFDE44]) were identified as its binding motif. Alanine substitutions in each domain rendered the ORF44F129A mutation lethal for VZV, similar to deletion of the entire ORF44. The phenotype of the ORF49-41AAAA44 mutation was comparable to that of the ORF49-defective virus, including small-plaque formation, impaired growth, and low infectious virus production. These results suggest that the interaction between ORF44 and ORF49 is essential for their role in VZV infection and that ORF49 is required for the efficient production of infectious progeny virus mediated by the conserved interaction between the two proteins.

Varicella-zoster virus (VZV) is a member of the human alphaherpesvirus subfamily and the etiologic agent of two diseases: varicella is the result of primary infection with VZV, and herpes-zoster is caused by reactivation of the virus from the latent state (1). VZV shares many features, especially a tropism for epithelial and neural tissues, with other human alphaherpesvirus members, including herpes simplex viruses 1 and 2 (HSV-1 and -2, respectively), and with the nonhuman alphaherpesviruses. However, VZV spreads only via cell-to-cell infection in culture and is more akin to the betaherpesviruses (i.e., human herpesviruses 6 and 7) in its apparent T-cell-tropism (1).

The VZV genome is approximately 125 kb and contains at least 70 unique open reading frames (ORFs), and it is the smallest genome in terms of length and gene set among human herpesviruses (1–3). Of the 70 identified ORFs, 44 are core genes that are conserved among all human herpesvirus subfamilies (4). Recent genome-wide mutagenesis analysis showed that 34 ORFs among the core genes are essential for virus reconstitution in cell culture, whereas deletion of seven ORFs results in viral growth defects, and three ORFs are dispensable in cell culture or skin organ culture (5). Eight core genes encode tegument proteins, which are the structural components of the virion and are located between the nucleocapsid and the envelope.

VZV ORF49 encodes a nonessential tegument protein that functions as a cell-tropic factor in cell culture via an unknown mechanism (6). VZV ORF49 is the homolog of HSV-1 UL11 and human cytomegalovirus (HCMV) UL99, which are among the most extensively studied tegument protein-encoding genes. The UL11 and UL99 gene products, pUL11 and pp28, function in secondary envelopment (7–9), but they have different roles in the viral life cycle. HSV-1 UL11 is not essential for the viral life cycle; however, the UL11 deletion mutant forms small plaques, and the final titers are reduced to 80 to 95% of wild-type levels (10). In contrast, HCMV UL99 is an essential gene, and pp28-deficient mutants show extremely impaired growth in normal fibroblasts and produce no detectable infectious progeny (9). However, this mutant spreads from cell to cell via an unknown mechanism (11).

Several recent reports, beginning with one on HSV-1 UL16, which is a core gene within the intron of a conserved herpesvirus spliced gene, (12), showed that interactions between pUL11 and pUL16 homologs were conserved beyond the host species and herpesvirus subfamilies (13–15). HSV pUL16 localizes to the nucleus and the cytoplasm of infected cells and functions in virus entry and in nuclear and cytoplasmic egress (16–19); pUL16 homologs may function in secondary envelopment, as reviewed in reference 20. As described for UL11 homologs, whether UL16 homologs are required for the viral life cycle differs among viruses (13, 15, 21–25). In a genome-wide mutagenesis analysis, deletion of the entire gene region from the viral genome of VZV ORF44, the UL16 homolog, showed that it is an essential gene by loss-of-function analysis in the MeWo cell line (5), although this was not

Received 11 August 2013 Accepted 10 October 2013
Published ahead of print 23 October 2013
Address correspondence to Yasuko Mori, ymori@med.kobe-u.ac.jp.
Copyright © 2014, American Society for Microbiology. All Rights Reserved.
doi:10.1128/JVI.02245-13

Downloaded from http://jvi.asm.org/ on December 18, 2013 by KOBE UNIVERSITY

confirmed by a revertant virus generated for gain-of-function analysis.

The LI motif and the conserved acidic cluster of pUL11 are essential for its interaction with pUL16 of HSV-1, whereas the critical sequences in pUL16 have not been determined because it is highly sensitive to deletions. Its short N-terminal 75-amino-acid (aa) fragment was recently shown to include the pUL11 binding site, and its C-terminal region functions as the binding regulatory domain (26), although this has not been confirmed in the context of HSV-1-infection. HCMV pUL94 directs pp28 to the assembly compartment, where it plays a role in secondary envelopment. Amino acids 37 to 39, near the acidic cluster of pp28, and one of the conserved cysteine residues of pUL94 are involved in binding in the context of infection (24, 27). In VZV, potential ORF49 protein (ORF49p)-binding proteins, including the pUL16 homolog ORF44 protein (ORF44p), were identified by global screening using the yeast two-hybrid system (28, 29), although these interactions have not been confirmed, even by coexpression experiments in mammalian cells.

In our previous study on VZV ORF49 (6), ORF49p was identified as one of the cell-tropic factors for VZV lytic infection in cell culture. However, the precise function of ORF49 in cells in which the ORF49-defective virus showed impaired growth was not elucidated. To address this issue, we established a complete *trans*-complementation system for ORF49 and identified ORF44p as its binding partner in the context of infection. In the present study, we aimed to reveal the precise role of ORF49p by using this system and by analyzing the conserved mechanism of interaction between these proteins and its role in VZV infection.

MATERIALS AND METHODS

Cells and viruses. The melanoma cell line MeWo was propagated in Dulbecco's modified Eagle's medium (DMEM) (Nissui Pharmaceutical, Ueno, Tokyo) supplemented with 8% fetal bovine serum (FBS) (Sigma-Aldrich, St. Louis, MO), 0.6 mg/ml L-sodium glutamate, and 0.02 mg/ml gentamicin sulfate (Nacalai Tesque, Kyoto, Japan) (DMEM complete). MeWo cells stably expressing Cre recombinase, designated MeWo-Cre cells, were maintained in DMEM complete supplemented with 500 μg/ml G418 (Nacalai Tesque) (30). MeWoORF49 cells stably expressing ORF49 were generated as follows: MeWo cells were transfected with CAG/ORF49 (described below) using Lipofectamine 2000 (Invitrogen, Carlsbad, CA) according to the manufacturer's instructions, selected, and propagated in DMEM complete supplemented with 1.5 μg/ml puromycin (Invitrogen). Recombinant viruses derived from the parental VZV strain Oka (pOka), rpOka, rpOkaΔ44Rev, rpOkaORF44F129ARev, rpOkaORF44T128A, rpOkaORF44K130A, rpOkaORF49M1L, rpOkaORF49M1LRev, rpOka-ORF49-41AAAA44, and rpOkaORF49-41AAAA44Rev were maintained in DMEM complete supplemented with 3% FBS.

Cell-free virus was prepared as described previously with slight modifications (6). At 48 h postinfection (hpi) by cell-to-cell spread, cells were harvested with a cell scraper (Iwaki, Tokyo, Japan), spun at 800 × *g* for 5 min at 4°C, and suspended in SGP buffer (phosphate-buffered saline [PBS] containing 0.1% L-sodium glutamate and 7% sucrose). The suspended cells were treated with an ultrasonic disruptor (UD-201; Tomy Seiko, Tokyo, Japan) at 1.5° for 30 s on ice and spun at 800 × *g* for 5 min at 4°C, and the supernatant was stored at −80°C until use. The purified viral particles were prepared as described in reference 6. Briefly, the cell-free virus solutions were subjected to Histodenz (Sigma-Aldrich) gradient purification (5 to 50% in PBS) by ultracentrifugation at 50,200 × *g* for 2 h at 4°C in a P40ST rotor (CP80WX; Hitachi Koki, Hitachinaka, Japan). Aliquots of the peak particle-containing fractions were subjected to ultracentrifugation at 52,600 × *g* for 2 h at 4°C in a P28S rotor (CP80WX; Hitachi Koki), and the pellets were stored at −80°C for further analyses.

Plasmids. The pGEX/ORF44, pGEX/ORF44A, and pGEX/ORF44P plasmids were generated to express the full length (corresponding to aa 2 to 363), anterior half (aa 2 to 200), and posterior half (aa 181 to 363) of the ORF44 protein in *Escherichia coli*. The primer pairs ORF44ecoF4 (5′-ACCGAATTCGAATTACAACGCATATTTCCG-3′) and ORF44salR (5′-ACCGTCGACCTAGGTGGTTGTAGG-3′) for ORF44, ORF44ecoF4 and ORF44salR600 (5′-ACCGTCGACTAAATTAGGTTCCATAGCC-3′) for ORF44A, and ORF44ecoF541 (5′-ACCGAATTCGGAGTGTGGTGGTCAGACG-3′) and ORF44salR for ORF44P were used to amplify each indicated region of the ORF44 gene from the rpOka cDNA. The PCR products were inserted in frame into the pGEX6P-1 bacterial expression vector (GE Healthcare Bio-Sciences, Piscataway, NJ) via the EcoRI and SalI sites (underlined). The same procedure was used to construct pGEX/ORF61. The DNA fragment (positions 406 to 744) of ORF61 was cloned into pGEX6P-1 via the BamHI and SalI sites (underlined). The primer pair was ORF61bamF406 (5′-ACCGGATCCGGGCCCCTTCAATCGTCGG-3′) and ORF61salR744stop (5′-ACCGTCGACCTAGAATCTCGCGTTTCCCTC-3′). The eukaryotic ORF44 expression plasmid CAG/ORF44 or CAG/FLAGORF44, which was N-terminally tagged with FLAG (DYKDDDDK), was generated as follows: the entire ORF44 gene was amplified by PCR with the primers ORF44-25kpnF (5′-ACCGGTACCAATCCGCTAGACTG-3′) or ORF44FLAGkpnF4 (5′-ACCGGTACCGCCACCATGgactacaaagacgatgacgacaagGAATTACAACGCATATTTCCG-3′) and ORF44salR, and the PCR fragment was cut by KpnI and SalI (underlined) and cloned into pCAGGS-MCS-neo via the KpnI and XhoI sites. The FLAG tag coding sequence within the primer for ORF44FLAGkpnF4 is shown in lowercase letters. The ORF49 expression plasmid CAG/ORF49 was generated as follows: the entire ORF49 gene was amplified by PCR with the primers ORF49-24ecoF (5′-ACCGAATTCTTACATCAGCATTGCG−3′) and ORF49bamR (5′-ACCGGATCCTTAACATTTTGCGCATTTGG-3′), and the PCR fragment was cut by EcoRI and BamHI (underlined) and cloned into pCAGGS-MCS-puro via the EcoRI and BglII sites. The pCAGGS plasmid was kindly provided by Jun-ichi Miyazaki (Osaka University, Japan) (31). A Cre recombinase-expressing plasmid, pCX-Cre-neo, was previously generated (30) from pCX-Cre, which was a generous gift from Masaru Okabe (Osaka University, Japan).

Construction of mutant ORF44 and ORF49 expression plasmids. The ORF44 mutant plasmids pGEX/ORF44F129A, CAG/ORF44T128A, CAG/ORF44F129A, CAG/ORF44K130A, CAG/FLAGORF44I121stop, CAG/FLAGORF44P136stop, and CAG/FLAGORF44F129AP136stop and the ORF49 mutant plasmid CAG/ORF49-41AAAA44 were generated with a QuikChange Lightning multisite-directed mutagenesis kit (Agilent Technologies, La Jolla, CA) according to the manufacturer's recommendations, using the primers listed in Table 1 based on pGEX/ORF44, CAG/ORF44, CAG/FLAGORF44, and CAG/ORF49, respectively. The ORF49 C-terminal deletion mutant plasmids CAG/ORF49N40, CAG/ORF49N44, and CAG/ORF49N48 were generated using the following primer pairs: ORF49-24ecoF (5′-ACCGAATTCTTACATCAGCATTGCG-3′) as the forward primer for all the deletion mutants and ORF49mycxhoR120 (5′-ACCCTCGAGcagatcctcttctgagatgagtttttgttcAAAGTCTTCAAAGAACTCTG-3′), ORF49mycxhoR132 (5′-ACCCTCGAGcagatcctcttctgagatgagtttttgttcCTCATCAAAGTCAAAGTCTT-3′), or ORF49mycxhoR144 (5′-ACCCTCGAGcagatcctcttctgagatgag tttttgttcCTCTGTTACATTCTCATCAAAGTC-3′) as the reverse primer for CAG/ORF49N40, CAG/ORF49N44, or CAG/ORF49N48. All of the reverse primers contained a c-myc tag, indicated by lowercase letters, and the PCR products were cloned into pCAGGS-MCS-puro via the EcoRI and XhoI sites (underlined).

Antibodies. To produce a mouse monoclonal antibody (MAb) against ORF44, a glutathione *S*-transferase (GST)-ORF44A recombinant protein was expressed in *E. coli* BL21 transformed with pGEX/ORF44A, purified, and used to immunize mice; hybridoma clones producing the anti-ORF44 MAb were established as described previously (32). To produce polyclonal anti-ORF61 Abs, a GST-ORF61 fusion protein was purified from *E. coli* BL21 transformed with pGEX-ORF61 and used to immunize a rabbit

Downloaded from http://jvi.asm.org/ on December 10, 2015 by INCOLL UNIVERSITY

TABLE 1 Primers used for ORF44 or ORF49 mutations

Primer	Sequence[a]	Amino acid substitution(s)
ORF44 361at-ta	5′-TAT CCG GTT GAA AAC TAA GAC CAT GTT TTT GGA-3′	Ile 121 to stop (TAA)
ORF44 382a-g	5′-CAT GTT TTT GGA GCA GCG TTT AAG AAC CC-3′	Thr 128 to Ala
ORF44 385tt-gc	5′-TT TTT GGA GCA ACG GCT AAG AAC CCG ATC G-3′	Phe 129 to Ala
ORF44 388aa-gc	5′-TTT GGA GCA ACG TTT GCG AAC CCG ATC GCG-3′	Lys 130 to Ala
ORF44 406ccc-taa	5′-AAC CCG ATC GCG TAC TAA CTT CCA ACA TCT ATT-3′	Pro 136 to stop (TAA)
ORF49 M1L	5′-ATT GCG GTC ATT GCG TTG GGA CAA TCT TCA-3′	Met 1 to Leu
ORF49 41AAAA44	5′-TTT GAA GAC TTT GCC GCT GCT GCG AAT GTA ACA GAG-3′	Asp-Phe-Asp-Glu (41–44) to Ala-Ala-Ala-Ala

[a] Nucleotides that differ from those of the wild type are underlined.

(Sigma Genosys, Hokkaido, Japan). The anti-ORF61 Ab was purified with GST-conjugated normal human serum (NHS)-activated Sepharose and GST-ORF61-conjugated NHS-activated Sepharose. Rabbit polyclonal anti-ORF49 and anti-gB-C Abs were described previously (6). The mouse anti-glycoprotein E (anti-gE) (clone 9) Ab was described in reference 33. Mouse anti-glycoprotein H (gH) (VgIII-3) was obtained as described previously (33). Sheep anti-*trans*-Golgi network (anti-TGN46) Ab (AHP500G; AbD Serotec, Oxford, United Kingdom), anti-α-tubulin Ab (B-5-1-2; Sigma-Aldrich), and goat anti-GST Ab (GE Healthcare Bio-Sciences) were commercially available. Alexa Fluor 488-labeled donkey anti-mouse immunoglobulin G (IgG), Alexa Fluor 594-labeled donkey anti-rabbit IgG, and Alexa Fluor 647-labeled donkey anti-sheep IgG (Invitrogen) were used as secondary Abs, and Hoechst 33342 (Sigma-Aldrich) was used for nuclear staining in confocal microscopic analyses. ECL enhanced chemiluminescence anti-mouse or anti-rabbit IgG horseradish peroxidase-linked whole antibodies from donkey (GE Healthcare Bio-Sciences) were used as secondary Abs in immunoblotting.

Mutagenesis of viral genomes in *E. coli*. The mutant bacterial artificial chromosomes (BACs) pOka-BACORF49M1L, containing a methionine-to-leucine substitution at residue Met-1, and pOka-BACORF49-41AAAA44, containing a tetra-alanine substitution at residues 41-Asp-Phe-Asp-Glu-44, were generated by *recA*-mediated allelic replacement in pOka-BAC-harboring DH10B transformed with pST76A-SR/pOkaORF49M1L and pST76A-SR/pOkaORF49-41AAAA44, respectively, which were derived from pST76A-SR/pOkaORF50 (including nucleotide positions 84361 to 89970 of pOka) (30), using the primers listed in Table 1 and a QuikChange Lightning multisite-directed mutagenesis kit. The revertant BACs pOka-BACORF49M1LRev and pOkaBACORF49-41AAAA44Rev were generated by recA-mediated allelic replacement using pST76A-SRORF50 transformed into DH10B cells harboring pOka-BACORF49M1L and pOka-BACORF49-41AAAA44, respectively.

To generate pOka-BACΔ44, in which the nucleotides (nt) 1 to 800 of the ORF44 gene were replaced with an FRT (*flp* recombinase recognition target) sequence, a linear fragment was amplified by PCR using the primer pair ORF44FRTfKMF0 (5′-TTAAACCCACAAGTACC CGGGCGGCAATCCGCTAGACTGTTTTTCTGCTCGAAGTTCCTA TTCTCTAGAAAGTATAGGAACTTCAGCAAGCGAACCGGAAT TGC-3′) and ORF44FRTrKMR800 (5′-TCCCGCTGACCGGCCTTT CTCCACATACACGGAGCCCAACACACACAACCGAAGTTCCTAT ACTTTCTAGAGAATAGGAACTTCCTTTTTCAATTCAGAAGA ACTC-3′) (FRT is underlined) using pCR2.1-TOPO as the template (Invitrogen). The amplified fragment was then transformed into DH10B harboring pOka-BAC (34) with pGETrec (a kind gift from Panayiotis A. Ioannou, The Murdoch Institute for Research into Birth Defects, Royal Children's Hospital, Melbourne, Australia) (35); *recE/T* recombination for pOka-BACΔ44KMr and excision of the kanamycin resistance gene from pOka-BACΔ44KMr by the *flp*/FRT system using pCP20 (a kind gift from Wilfried Wackernagel, Universität Oldenburg, Germany) (36), resulting in pOka-BACΔ44, were carried out as described previously (6).

To construct pOka-BACΔ44Rev, the revertant BAC genome against pOka-BACΔ44, *recA*-mediated mutagenesis was performed as described previously (30), using the shuttle plasmid pST76A-SR/pOkaORF44. For pST76A-SR/pOkaORF44, a 3.2-kbp fragment of viral DNA corresponding to nt 79230 to 82453 of pOka was amplified from the pOka-BAC genome using the primer pair ORF43F1201 (5′-ACCGCTGCGTGTATA AATGCCCGGGTTGAC-3′) and ORF42/45F (5′-ACCATGTCATTGAT AATGTTTGG-3′), cloned into pCR2.1-TOPO, sequenced, cut with EcoRI, blunted, and cloned into the plasmid pST76A-SR (kindly provided by Ulrich H. Koszinowski, Max von Pettenkofer Institut, Ludwig-Maximilians-Universität München, Munich, Germany) (37), which was cut with KpnI and blunted.

The shuttle plasmids for the ORF44 point mutant BACs, pST76A-SRORF44T128A (with an alanine substitution for threonine at residue Thr-128), pST76A-SR/pOkaORF44F129A (with an alanine substitution for phenylalanine at residue Phe-129), and pST76A-SR/pOkaORF44K130A (with an alanine substitution for lysine at residue Lys-130), were generated from pST76A-SR/pOkaORF44 with a QuikChange Lightning multisite-directed mutagenesis kit using the primers listed in Table 1. Each mutated shuttle plasmid was transformed into DH10B harboring pOka-BACΔ44KMr, and *recA*-mediated allelic replacement was performed as described elsewhere (30) to generate pOka-BACORF44T128A, pOka-BACORF44F129A, and pOka-BACORF44K130A. The revertant BAC for the ORF44F129A mutant BAC, pOka-BACORF44F129ARev, was generated by *recA*-mediated allelic replacement using pST76A-SRORF44 transformed into pOka-BACORF44F129A-harboring DH10B.

All of the purified BACs were digested with BamHI or EcoRI to ensure that the expected DNA fragments were present, and the whole region for allelic replacement was sequenced to ensure that unexpected deletions or substitutions were not present.

Reconstitution of recombinant viruses and excision of the BAC cassette. MeWo cells or MeWoORF49 cells for rpOkaORF49M1L and rpOkaORF49-41AAAA44 seeded in one well of a 12-well plate were transfected with 3 μg of BAC DNA using Lipofectamine 2000 or X-treamGene HP (Roche Applied Science, Basel, Switzerland). After typical cytopathic effects (CPE) were seen in cells expressing green fluorescent protein (GFP), cell-free virus was prepared as described above and used to infect MeWo-Cre cells or pCX-Cre-neo-transfected MeWoORF49 cells for rpOkaORF49M1L and rpOkaORF49-41AAAA44 to excise the BAC cassette.

Immunoblotting, immunoprecipitation, and immunofluorescence. Immunoblotting, immunoprecipitation, and immunofluorescence were performed as described previously (30, 32) with slight modifications. The proteins in immunoblots were visualized by Chemi-Lumi One Super (Nacalai Tesque) in combination with LAS4000mini (GE Healthcare Bio-Sciences). Radioimmunoprecipitation assay (RIPA) lysis buffer (0.01 M Tris-HCl [pH 7.4], 0.15 M NaCl, 1% sodium deoxycholate, 1% Nonidet P-40, 0.1% SDS, 1 mM EDTA) supplemented with protease inhibitor cocktail (Sigma-Aldrich) was used for cell lysis, and the supernatants obtained by ultracentrifugation at 216,900 × *g* for 1 h at 4°C in a P50A3 rotor (CP80WX; Hitachi Koki) and precleared with protein G Sepharose 4 Fast Flow (GE Healthcare Bio-Sciences) were used for immunoblotting and immunoprecipitation. Immunofluorescence images were captured and analyzed by an FV1000D confocal microscope (Olympus, Tokyo, Japan).

Downloaded from http://jvi.asm.org/ on December 18, 2013 by KOBE UNIVERSITY

***In vitro* binding assay.** To analyze the interaction of GST-ORF44 with ORF49, GST-ORF44, GST-ORF44F129A, or GST-ORF44P recombinant protein was expressed in and purified using BugBuster master mix (Merck Millipore, Darmstadt, Germany) from *E. coli* BL21 transformed with pGEX/ORF44, pGEX/ORF44F129A, or pGEX/ORF44P as described above. ORF49p was expressed in MeWo cells by transfection of CAG/ORF49 using Lipofectamine 2000 and solubilized as described above. GST-ORF44 recombinant protein was bound to glutathione Sepharose 4B (GE Healthcare Bio-Sciences) overnight at 4°C, washed with PBS three times, pelleted, and reacted with soluble ORF49p overnight at 4°C. The bead–GST-ORF44 recombinant protein–ORF49p complex was washed with RIPA lysis buffer three times, pelleted, suspended in SDS-PAGE sample buffer, boiled, and subjected to SDS-PAGE and immunoblotting as described above.

Protein identification by MS. MeWo cells were infected with pOka by cell-to-cell infection and lysed with RIPA lysis buffer as described above. The cell lysates from pOka- or mock-infected MeWo cells were precleared with protein G Sepharose and subjected to immunoprecipitation with anti-ORF49 Ab cross-linked protein G Sepharose. The immunoprecipitates were separated by SDS-PAGE and stained with a SilverQuest silver staining kit (Invitrogen). Protein bands were excised from the gel and digested with trypsin (sequencing grade; Promega, Madison, WI) according to published procedures (38). Nano-liquid chromatography-tandem mass spectrometry (nano-LC-MS/MS) analyses were performed on an LTQ-Orbitrap XL mass spectrometer (Thermo Fisher Scientific, Waltham, MA) equipped with a nano-electrospray ionization (nano-ESI) source (AMR, Tokyo, Japan) and coupled to a Paradigm MG4 pump (Michrom Bioresources, Auburn, CA) and autosampler (HTC PAL; CTC Analytics, Zwingen, Switzerland). A spray voltage of 1,800 V was applied. The peptide mixture was separated on a Magic C_{18} AQ column (100 μm by 150 mm, 3.0-μm particle size, 300 Å; Michrom Bioresources) with a flow rate of 500 nl/min. The linear gradient was as follows: 5% to 45% B in 30 min, 45% to 95% B in 0.1 min, 95% B for 2 min, and finally 5% B (solvent A = 0.1% formic acid in 2% acetonitrile, and B = 0.1% formic acid in 90% acetonitrile). Intact peptides were detected in the Orbitrap at a resolution of 60,000. For the LC-MS/MS analysis, six precursor ions were selected for subsequent MS/MS scans in a data-dependent acquisition mode following each full scan (*m/z*, 350 to 1,500). A lock mass function was used for the LTQ-Orbitrap to obtain constant mass accuracy during the gradient analysis. Peptides and proteins were identified by automated database searches using Proteome Discoverer v.1.1 (Thermo Fisher Scientific, Waltham, MA) against human entries or all entries of the Swiss-Prot protein database (version 3.26) with a precursor mass tolerance of 10 parts per million (ppm), a fragment ion mass tolerance of 0.8 Da, and strict trypsin specificity, allowing for up to two missed cleavages. Cysteine carbamidomethylation was set as a fixed modification, and methionine oxidation was allowed as a variable modification.

Plaque size and infectious-center assays for growth kinetics. To analyze the growth kinetics of the recombinant viruses, infectious-center assays were performed as described previously (6) with slight modifications. Briefly, 5×10^5 MeWo or MeWoORF49 cells were seeded on one well of a 12-well plate and inoculated with 50 PFU of cell-free virus per well. For the plaque size measurement, the infected cells were cultured for 7 days. For the infectious-center assay, infected cells were harvested at 24-h intervals and then titrated on newly prepared cells. The cells were fixed in 30% methanol and 70% acetone and stained with an anti-gE MAb (clone 9) and secondary ECL anti-mouse IgG horseradish peroxidase-linked whole antibody (GE Healthcare Bio-Sciences). The stain was developed with 3,3′,5,5′-tetramethylbenzidine-H (TMB-H) peroxidase substrate (Moss, Inc., Pasadena, MD). Images of the plaques were captured and traced, and the number of plaques was counted, or the plaque area was measured using ImageJ (http://rsbweb.nih.gov/ij/).

RESULTS

ORF49 functions in the efficient production of infectious progeny virus. To examine the mechanism of action of ORF49, we performed loss-of-function and gain-of-function analyses by generating an ORF49-defective virus, rpOkaORF49M1L, and its revertant virus, rpOkaORF49M1LRev, from the pOka-BACORF49M1L and pOka-BACORF49M1LRev genomes, respectively (Fig. 1A and C). In addition, the MeWoORF49 cell line was established to express ORF49 constitutively in MeWo cells in which the previous ORF49-defective virus, rpOkaΔ49, specifically showed an impaired growth phenotype (6), and gain-of-function analysis was performed by ORF49 *trans*-complementation assay.

None of the assayed viral proteins, including glycoprotein H (gH), ORF61 protein (ORF61p), ORF44p, and ORF49p, were detected in MeWo cells (Fig. 2A, lane 1). In MeWoORF49 cells, ORF49p was the only protein detected among the tested viral proteins (Fig. 2A, lane 2), and its expression level was comparable to that of ORF49p in rpOka-infected MeWo cells (Fig. 2A, lane 3). In rpOkaORF49M1L-infected cells, ORF49p was not detected in the infected MeWo cells (Fig. 2A, lane 4) or in the viral particles (Fig. 2C, lane 2), although gH and ORF61p were clearly expressed in infected cells (Fig. 2A, lane 4), as was gH in the viral particles (Fig. 2C, lane 2). The rpOkaORF49M1LRev line expressed all of the viral proteins tested (Fig. 2A, lane 5), similar to rpOka-infected MeWo cells (Fig. 2A, lane 3).

To confirm the ORF49-defective phenotype and perform gain-of function analysis, plaque formation was analyzed on MeWo and MeWoORF49 cells (Fig. 3A). Plaque sizes were similar between rpOka-infected MeWo and MeWoORF49 cells (Fig. 3A, lanes 1 and 2), indicating that the exogenous expression of ORF49 had neither positive nor negative effects on normal VZV infection. Similar to our previous results using rpOkaΔ49, rpOkaORF49M1L formed significantly smaller plaques on MeWo cells (Fig. 3A, lane 3) than on MeWoORF49 cells, and this reduction was recovered in the revertant virus infection in MeWo cells (Fig. 3A, lane 5) and completely rescued by the exogenous expression of ORF49 in MeWoORF49 cells (Fig. 3A, lane 4). Consistent with the plaque formation assay results, rpOkaORF49M1L propagated on MeWo cells showed slower growth than rpOka or rpOkaORF49M1LRev on MeWo or MeWoORF49 cells in an infectious-center assay, and the growth impairment of rpOkaORF49M1L was completely rescued by exogenous ORF49p in MeWoORF49 cells (Fig. 3B).

During the preparation of cell-free viruses, another strikingly different phenotype of the ORF49 defect was observed. As summarized in Table 2, the titer of cell-free virus or plaque size formed by the cell-free virus infection of rpOka was almost the same whether the virus was propagated on MeWo or MeWoORF49 cells or titrated on MeWo or MeWoORF49 cells, again indicating that the exogenous ORF49p had no effect on normal VZV infection. When rpOkaORF49M1L was propagated on MeWo cells, the titer of cell-free virus was 3 to 5% of that observed with propagation of MeWoORF49 cells, and the plaque size depended on the kind of cells used for titration but not on the kind used for propagation. In addition, the rpOkaORF49M1L particles isolated from MeWoORF49 cells contained abundant ORF49p (Fig. 2C, lane 3) and produced almost the same titer of cell-free virus as the parental virus but formed significantly smaller plaques on MeWo cells (Table 2). This gain-of-function analysis performed using the ORF49 *trans*-complementation system suggested that the incom-

Downloaded from http://jvi.asm.org/ on December 19, 2013 by KOBE UNIVERSITY

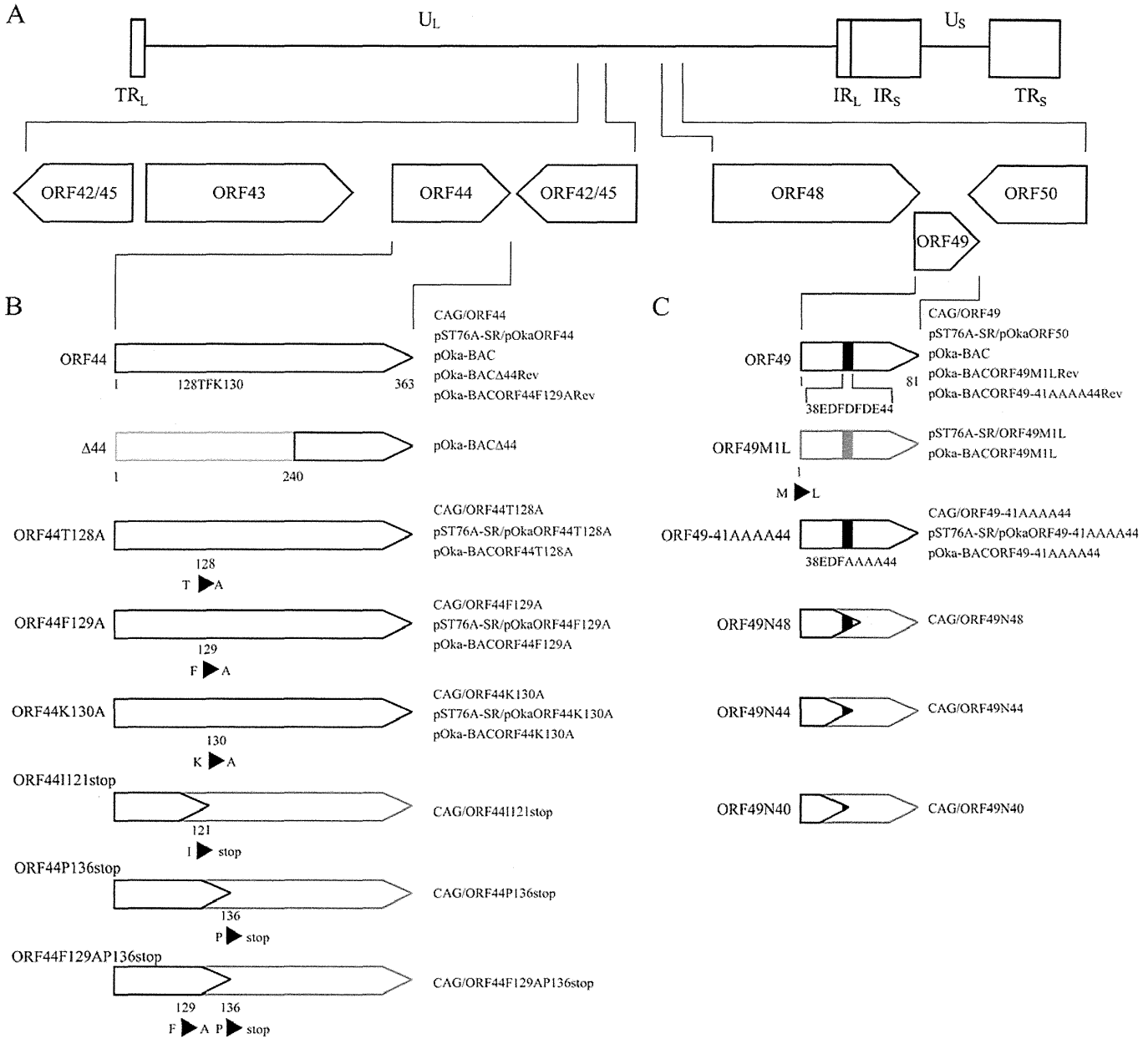


FIG 1 Schematics showing the plasmids and recombinant BAC genomes for ORF44 and ORF49. (A) Location of the ORF44 and ORF49 genes in the unique long region (U_L) segment of the genome of VZV strain pOka; terminal repeats (TR), unique short region (U_S), and internal repeats (IR) are indicated. (B) The wild type, deleted Δ44 region, and amino acid substitutions in ORF44p are shown. (C) The wild type, amino acid substitutions at the first methionine or the carboxyl-terminal half of the acidic cluster from amino acid positions 41 to 44, and the carboxyl-terminal truncations within ORF49p are shown. The acidic cluster is indicated as a black box. (B and C) Unexpressed regions of the mutant proteins are shown in gray outlined shapes. The names of relevant BACs, shuttle plasmids, and mammalian expression plasmids containing mutations are shown on the right.

ing ORF49p from the viral particles into the cells was not functional in any step and revealed that *de novo* ORF49p functioned in the production of infectious progeny viruses required for efficient propagation.

Furthermore, to examine the role of ORF49 in the production of infectious progeny viruses in detail, we redesigned our study on ORF49 to investigate its function by analyzing its binding partners.

Identification of the ORF44 protein as the binding partner for ORF49. ORF49p was immunoprecipitated from pOka- or mock-infected MeWo cells using an anti-ORF49 antibody (Ab), and the coimmunoprecipitating proteins were separated in a denaturing gel and visualized by silver staining (Fig. 4A). An approximately 36-kDa band was coimmunoprecipitated with the 13-kDa band corresponding to the ORF49p in pOka-infected MeWo cell lysates (Fig. 4A, lane 1). This 36-kDa band was identified as the ORF44 protein (ORF44p) of VZV by LC-MS/MS analysis (24.3% coverage of 363 amino acids).

ORF44p was specifically detected as a 36-kDa band in all recombinant VZV-infected MeWo cells, including rpOkaORF49M1L, by

Downloaded from http://jvi.asm.org/ on December 18, 2013 by KOBE UNIVERSITY

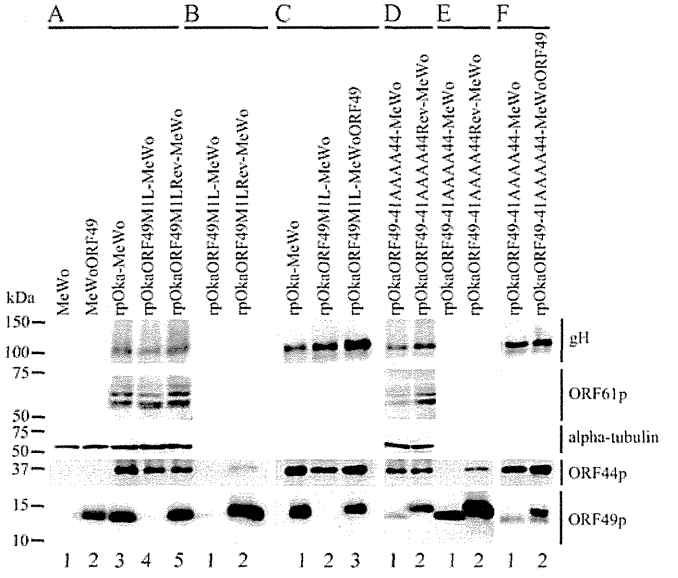


FIG 2 Expression and interaction of viral proteins during ORF49 mutant virus infection. (A) Proteins expressed in mock-infected MeWo cells (lane 1), mock-infected MeWoORF49 cells (lane 2), rpOka-infected MeWo cells (lane 3), rpOkaORF49M1L-infected MeWo cells (lane 4), and rpOkaORF49M1LRev-infected MeWo cells (lane 5) were visualized with Abs against gH, ORF61p, α-tubulin, ORF44p, and ORF49p. (B) The interaction between ORF44p and ORF49p was analyzed in rpOkaORF49M1L-infected cells (lane 1) and rpOkaORF49M1LRev-infected cells (lane 2). Immunoprecipitates obtained with an anti-ORF49 Ab from each type of virus-infected cells were electrophoretically separated and visualized using anti-ORF44 and anti-ORF49 Abs. (C) The viral proteins incorporated into virions from rpOka-infected MeWo cells (lane 1), rpOkaORF49M1L-infected MeWo cells (lane 2), and rpOkaORF49M1L-infected MeWoORF49 cells (lane 3) were visualized using Abs against gH, ORF61p, ORF44p, and ORF49p. (D) Proteins expressed in rpOkaORF49-41AAAA44-infected MeWo cells (lane 1) and rpOkaORF49-41AAAA44Rev-infected MeWo cells (lane 2) were visualized using Abs against gH, ORF61p, α-tubulin, ORF44p, and ORF49p. (E) The interaction between ORF44p and ORF49p was analyzed in rpOkaORF49-41AAAA44-infected cells (lane 1) and rpOkaORF49-41AAAA44Rev-infected cells (lane 2). Immunoprecipitates obtained using an anti-ORF49 Ab from each type of virus-infected cells were electrophoretically separated and visualized with anti-ORF44 and anti-ORF49 Abs. (F) The viral proteins incorporated into virions from rpOkaORF49-41AAAA44-infected MeWo cells (lane 1), and rpOka-ORF49-41AAAA44-infected MeWoORF49 cells (lane 2) were visualized with Abs against gH, ORF61p, ORF44p, and ORF49p.

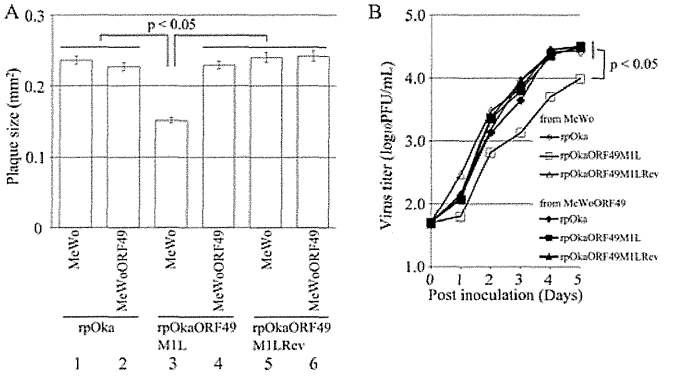


FIG 3 Growth properties of the ORF49M1L mutant virus in MeWo and MeWoORF49 cells. (A) Comparison of plaque sizes among recombinant viruses. MeWo cells or MeWoORF49 cells were infected with rpOka, rpOkaORF49M1L, or rpOkaORF49M1LRev (50 PFU/well) and cultured for 7 days. The infected cells were then stained with an anti-gE Ab, and the plaques were traced and measured by ImageJ software. Plaque size is shown with the standard error of the mean. Statistical significance was determined by Student's *t* test. (B) Growth kinetics of recombinant viruses in MeWo and MeWoORF49 cells. MeWo or MeWoORF49 cells were infected with rpOka, rpOkaORF49M1L, or rpOkaORF49M1LRev (50 PFU/well), harvested at the indicated times, serially diluted, added to newly prepared MeWo cells, and cultured for 5 days. The plaques were stained with an anti-gE Ab and counted. Each point represents the mean titer for two wells of one experiment. The experiments were performed twice independently. Statistical significance was determined by Student's *t* test.

immunoblotting with an anti-ORF44 Ab (Fig. 2A, lanes 3, 4, and 5). ORF44p was coimmunoprecipitated with ORF49p only in cells infected with the wild-type virus, rpOka, or rpOkaORF49M1LRev (data not shown) (Fig. 2B, lane 2) but not in the absence of ORF49p, as seen in rpOkaORF49M1L infection (Fig. 2B, lane 1). Thus, the interaction of ORF44p and ORF49p was specific and conserved in VZV.

ORF44 is essential for viral growth in cell culture. Because ORF49 is completely dispensable for viral reconstitution and propagation in MRC-5 cells, and the interaction between ORF44p and ORF49p was confirmed, we predicted that the ORF44 deletion mutant would be viable at least in MRC-5 cells, despite the fact that loss-of-function analysis showed that it is essential in MeWo cells (5). The ORF44 deletion mutant virus could not be reconstituted from pOka-BACΔ44 (Fig. 1B) in either MeWo cells or MRC-5 cells; however, the revertant virus of pOka-BACΔ44 reconstituted from the pOka-BACΔ44Rev genome (Fig. 1B) showed almost the same plaque size and growth as the parental virus, rpOka, in MeWo cells (data not shown). These findings confirmed that ORF44 is essential for VZV growth in cell culture even in MRC-5 cells.

ORF44p binds to and depends on ORF49p for its accumulation on the TGN in coexpressing cells and infection. When ORF44p was expressed alone by CAG/ORF44 transfection, it was dispersed throughout the cytoplasm and did not localize to the TGN (Fig. 5A). When ORF49p was expressed alone, it was predominantly localized to the juxtanuclear region with TGN46 (Fig. 5B), as reported previously (6). In cells coexpressing ORF44 and ORF49, ORF44p accumulated on the TGN with ORF49p (Fig. 5C), suggesting that the complex formation between ORF44p and ORF49p required no other viral factors and that it functioned in the accumulation of the ORF44p on the TGN. The expression of and interaction

TABLE 2 Comparison of cell-free virus titer and plaque formation

Virus	Cells for: Propagation	Titration	Titer (PFU/ml)[a]	Mean (SE) plaque size, mm²[b]
rpOka	MeWo	MeWo	2.3×10^3	0.232 (0.00891)
	MeWo	MeWoORF49	4.1×10^3	0.225 (0.00854)
	MeWoORF49	MeWo	4.0×10^3	0.232 (0.00911)
	MeWoORF49	MeWoORF49	1.3×10^3	0.206 (0.00828)
rpOkaORF49M1L	MeWo	MeWo	1.5×10^2	0.161 (0.00601)
	MeWo	MeWoORF49	1.7×10^2	0.235 (0.01319)
	MeWoORF49	MeWo	4.0×10^3	0.147 (0.00534)
	MeWoORF49	MeWoORF49	6.3×10^3	0.228 (0.01474)
rpOkaORF49-41AAAA44	MeWo	MeWo	1.2×10^2	0.141 (0.00726)
	MeWo	MeWoORF49	1.3×10^2	0.212 (0.00669)
	MeWoORF49	MeWo	2.1×10^3	0.149 (0.00796)
	MeWoORF49	MeWoORF49	4.7×10^3	0.227 (0.00740)

[a] Titers of cell free viruses are shown from one experiment performed in duplicate.
[b] Plaque sizes are shown as means (standard errors [SE]) from one experiment performed in duplicate.

Downloaded from http://jvi.asm.org/ on December 19, 2015 by NCDC UNIVERSITY

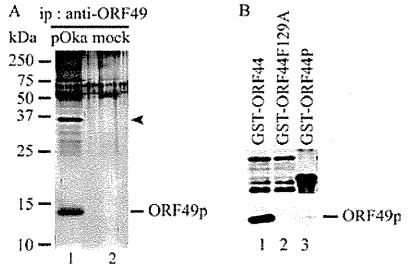


FIG 4 Identification of ORF44p as the binding partner of ORF49p by proteomic analysis and their *in vitro* binding assay. (A) pOka-infected MeWo cells expanded by cell-to-cell spread with full CPE at 2 to 3 days postinfection were lysed with RIPA buffer, and the binding molecules were coimmunoprecipitated with ORF49p using an anti-ORF49 Ab (lane 1). Mock-infected MeWo cells were used as a negative control (lane 2). The immunoprecipitates (ip) were electrophoretically separated and visualized by silver staining. (B) ORF49p expressed in and purified from MeWo cells was incubated with purified GST-ORF44 (lane 1), GST-ORF44F129A (lane 2), or GST-ORF44P (lane 3). Bound proteins were electrophoretically separated and visualized by anti-GST Abs (upper panel) and anti-ORF49 Abs (lower panel).

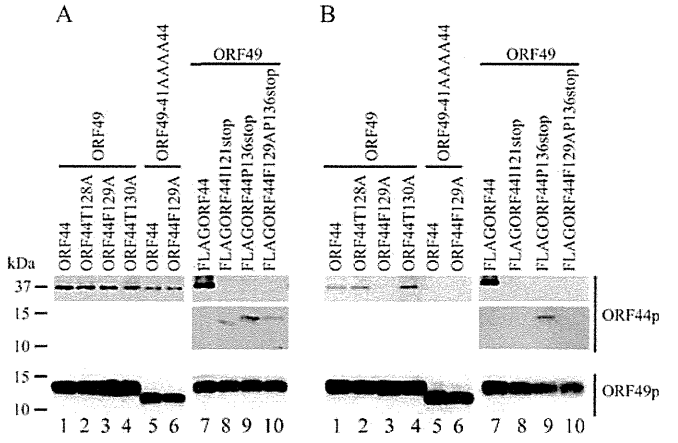


FIG 6 Expression and interaction of ORF44p and ORF49p in cotransfected cells. MeWo cells were cotransfected with CAG/ORF49 (lanes 1 to 4 and 7 to 10) or CAG/ORF49-41AAAA44 (lanes 5 and 6) and CAG/ORF44 (lanes 1 and 5), CAG/ORF44T128A (lane 2), CAG/ORF44F129A (lanes 3 and 6), CAG/ORF44K130A (lane 4), CAG/FLAGORF44 (lane 7), CAG/FLAGORF44I121stop (lane 8), CAG/FLAGORF44P136stop (lane 9), or CAG/FLAGORF44F129AP136stop (lane 10) (A and B). Protein expression was visualized with anti-ORF44p and anti-ORF49p antibodies (A), and proteins immunoprecipitated by anti-ORF49 Ab from cotransfected cells were electrophoretically separated and visualized using anti-ORF44 and anti-ORF49 Abs (B).

between ORF44p and ORF49p were confirmed by immunoblotting with the corresponding Abs and immunoprecipitation with anti-ORF49 Ab followed by immunoblotting with each Ab (Fig. 6A, lane 1, and B, lane 1, respectively). In rpOkaORF49M1LRev-infected MeWo cells, in spite of the broadly diffuse pattern seen for ORF44p, it appeared to accumulate on the TGN with ORF49p (Fig. 7B), as was seen in coexpressing cells (Fig. 5C), and this pattern was also observed in cells infected with rpOka (data not shown). In rpOkaORF49M1L-infected cells, ORF44p was dispersed as in cells expressing ORF44 alone and was not accumulated on the TGN (Fig. 7A), again indicating that the accumulation of ORF44p on the TGN depended on ORF49p and required no other viral factors.

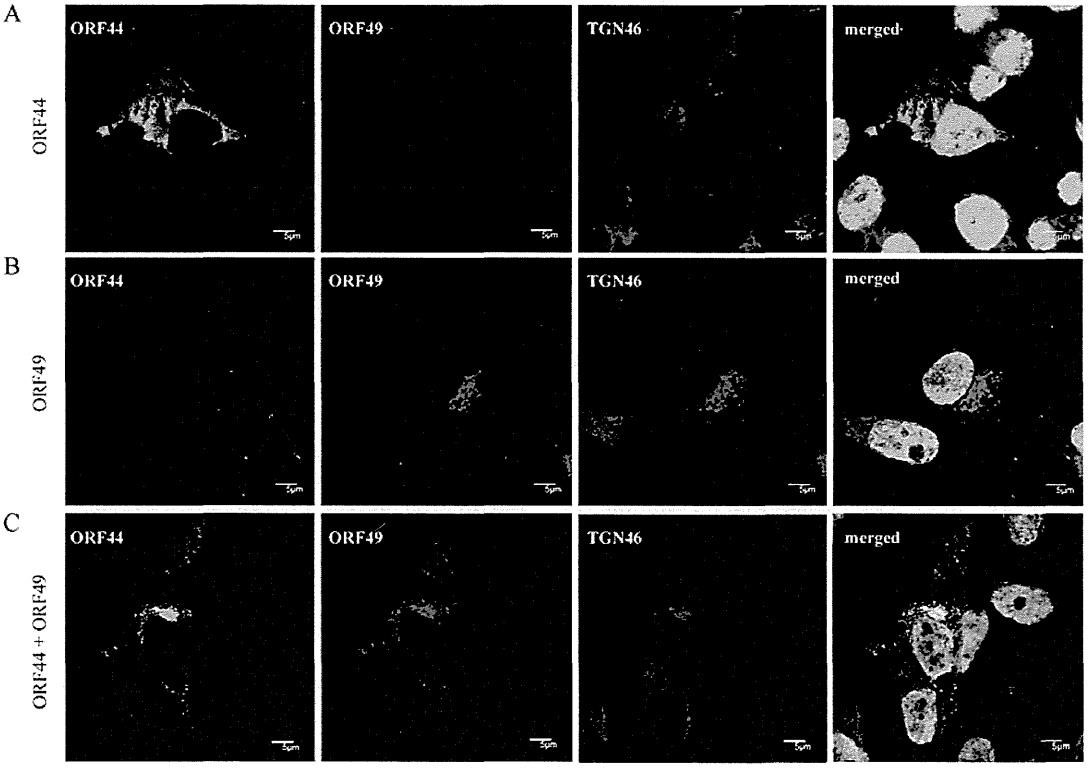


FIG 5 Localization of ORF44p and ORF49p in transiently transfected MeWo cells. MeWo cells were transfected with CAG/ORF44 (A) or CAG/ORF49 (B) or cotransfected with CAG/ORF44 and CAG/ORF49 (C). Cells were fixed at 48 h posttransfection and triple labeled for ORF44p (green), ORF49p (red), and TGN46 (blue). Nuclei were stained with Hoechst 33342 (cyan). Scale bars, 5 μm.

Downloaded from http://jvi.asm.org/ on December 18, 2013 by KOBE UNIVERSITY

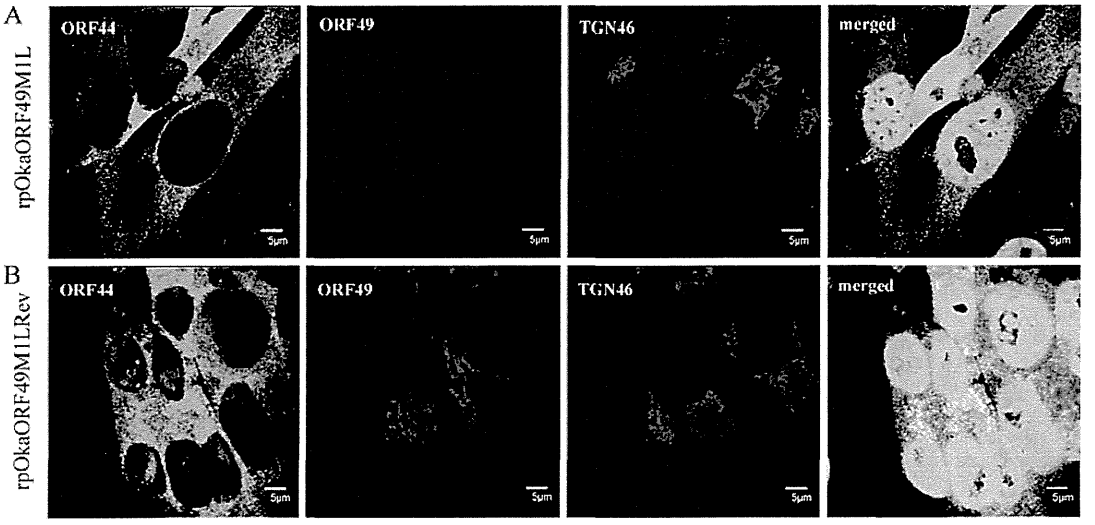


FIG 7 Localization of ORF44p and ORF49p in rpOkaORF49M1L-infected MeWo cells. rpOkaORF49M1L-infected (A) and rpOkaORF49M1LRev-infected (B) MeWo cells were fixed at 48 hpi and triple labeled for ORF44p (green), ORF49p (red), and TGN46 (blue). Nuclei were stained with Hoechst 33342 (cyan). Scale bars, 5 μm.

The phenylalanine at amino acid position 129 of ORF44p functions in the conserved interaction and is essential for VZV infection. In the process of ORF44 cloning, one mutant showed a T-to-C substitution at nt 385, which led to a phenylalanine-to-serine transition at aa 129 (F129S). In cells coexpressing ORF44F129Sp and ORF49p, ORF44F129Sp did not accumulate on the TGN and was not coimmunoprecipitated with ORF49p (data not shown).

To examine whether 129F functions specifically in the conserved interaction in VZV, alanine scanning was performed around 129F (Fig. 1B). ORF44T128Ap, ORF44F129Ap, and ORF44K130Ap showed similar distributions, and none of these mutants localized to the TGN when expressed alone (data not shown), as observed in cells expressing ORF44p alone (Fig. 5A). Coexpression of ORF44T128Ap and ORF44K130Ap with ORF49p (Fig. 8A and C, respectively) resulted in their colocalization with ORF49p at the TGN, as observed in cells coexpressing ORF44p and ORF49p (Fig. 5C). In contrast, ORF44F129Ap was dispersed throughout the cytoplasm and failed to accumulate on the TGN, even when coexpressed with ORF49p (Fig. 8B). The levels of expression of ORF44T128Ap, ORF44F129Ap, and ORF44K130Ap were almost equal (Fig. 6A, lanes 2, 3, and 4, respectively), and ORF44T128Ap and ORF44K130Ap were coimmunoprecipitated with ORF49p (Fig. 6B, lanes 2 and 4, respectively), whereas ORF44F129Ap was not coimmunoprecipitated with ORF49p (Fig. 6B, lane 3).

The results for F129S and F129A suggest that the binding site for ORF49p might reside in an N-terminal domain, as was recently reported for the pUL16 of HSV-1 (26). Therefore, stop codons were inserted at positions to either side of codon 129F (i.e., at I121stop and P136stop). In addition, a construct containing both the F129A and P136stop mutations was made (Fig. 1B). All three mutants were expressed at their predicted size (Fig. 6A, lanes 8, 9, and 10), and only the ORF44P136stop protein was coimmunoprecipitated with ORF49p (Fig. 6B, lane 9), whereas the ORF44I121stop and ORF44F129AP136stop proteins were not (Fig. 6B, lanes 8 and 10, respectively). Consistent with this, only the ORF44P136stop protein accumulated on the TGN with ORF49p (Fig. 8E), and the other two mutants did not (Fig. 8D and F), despite the diffused cytoplasmic localization of all mutants if expressed alone (data not shown). These results show that the binding site for ORF49p resides in the first third of ORF44p and that 129F plays a critical role in binding, either directly or indirectly. Furthermore, in GST-pulldown assays using GST-ORF44 (corresponding to aa 2 to 363), GST-ORF44F129A (aa 2 to 363 with F129A mutation), and GST-ORF44P (aa 180 to 363), only GST-ORF44 pulled down ORF49p expressed in and purified from MeWo cells (Fig. 4B), suggesting that there may not be a binding site within the C-terminal half of ORF44p; however, other C-terminal constructs have not been tested in this or other assays.

To analyze the impact of the 129F mutation in the context of infection, pOka-BACORF44T128A, pOka-BACORF44F129A, pOka-BACORF44K130A, and the revertant BAC for pOka-BACORF44F129A, pOka-BACORF44F129ARev, were generated (Fig. 1B). With the exception of the ORF44F129A mutant, the reconstitution of each virus with a mutation around 129F and of the revertant virus for the F129A mutant was successful, and all of the reconstituted viruses showed similar growth to rpOka (data not shown), suggesting that 129F of ORF44p may play a central role in the function of ORF44p in VZV infection, which occurs through its interaction with ORF49p.

The carboxyl-terminal half of the acidic cluster of ORF49p is required for the conserved interaction with ORF44p. To map the binding domain of ORF49p for ORF44p using the accumulation of ORF44p as an indicator of the interaction, we generated a series of carboxyl-terminal-truncated mutants of ORF49p (Fig. 1C). The coexpression of ORF44p and ORF49N48p or ORF49N44p resulted in the accumulation of ORF44p at the juxtanuclear region with TGN46 and the mutant ORF49p (Fig. 9A and B). In contrast, ORF44p never colocalized with ORF49N40p (Fig. 9C) and was dispersed in the cytoplasm, as when it was expressed alone (Fig. 5A). These results suggested that the ORF44p-binding domain in ORF49p may be located between the aspartate at aa 41 and glutamate at aa 44, which is in the carboxyl-terminal half of the conserved acidic cluster (Fig. 1C) in the ORF49 homologs.

Downloaded from http://jvi.asm.org/ on December 19, 2015 by NCCT UNIVERSITY

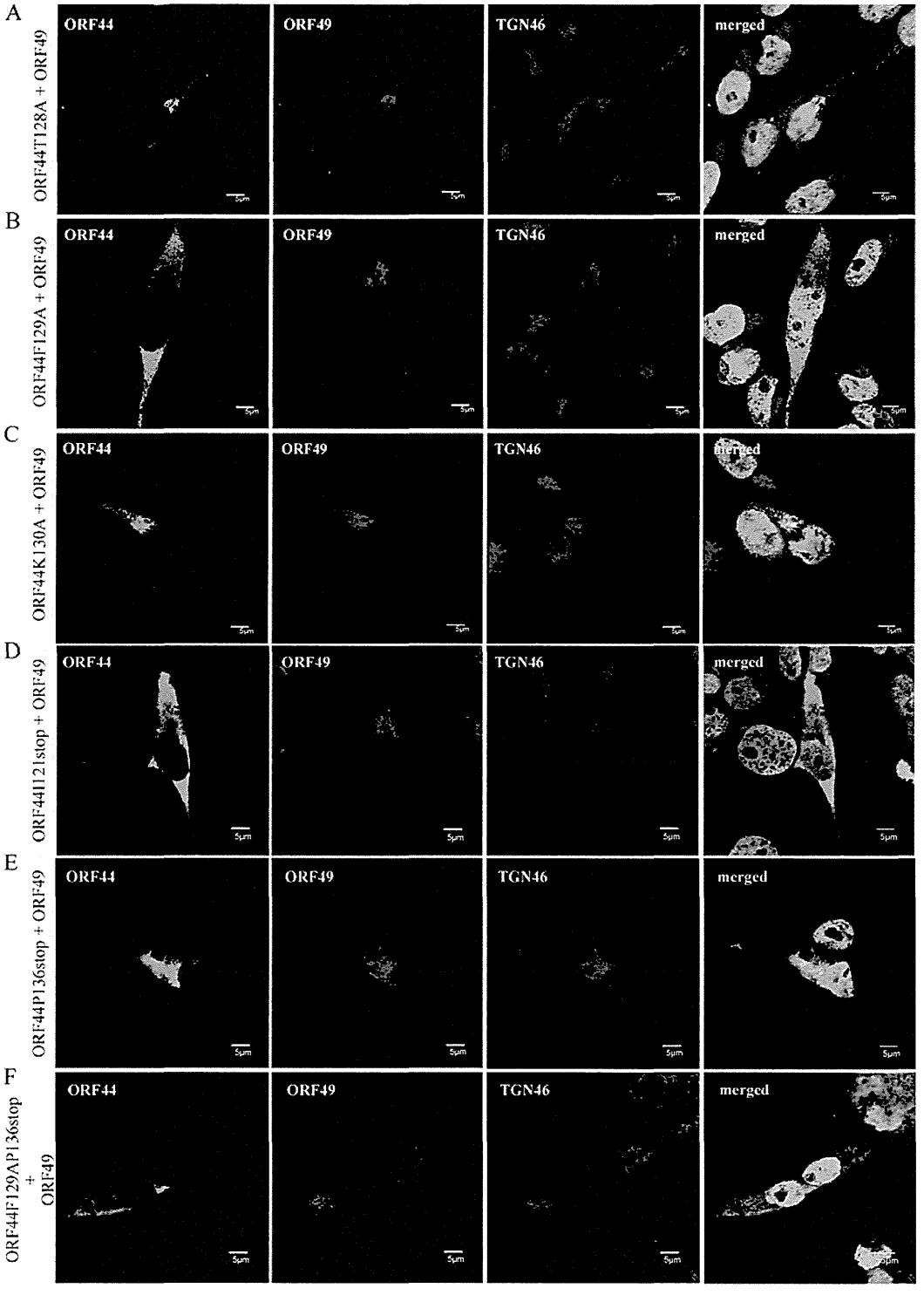


FIG 8 Localization and accumulation of ORF44 mutant proteins in MeWo cells expressing ORF49p. MeWo cells were cotransfected with CAG/ORF49 and CAG/ORF44T128A (A), CAG/ORF44F129A (B), CAG/ORF44K130A (C), CAG/FLAGORF44I121stop (D), CAG/FLAGORF44P136stop (E), or CAG/FLAGORF44F129AP136stop (F). Cells were fixed at 48 h posttransfection and triple labeled for ORF44 (green), ORF49 (red), and TGN46 (blue). Nuclei were stained with Hoechst 33342 (cyan). Scale bars, 5 μm.

To confirm the specificity of the ORF44p and ORF49p interaction while avoiding (although not excluding) nonspecific effects on the function of ORF49p resulting from the destruction of the ORF49p backbone, the four residues (41DFDE44) identified as the candidate ORF44p-binding motif were replaced by alanine, resulting in ORF49-41AAAA44p (Fig. 1C). As shown in Fig. 9D, ORF49-41AAAA44p targeted the TGN, similar to ORF49p (Fig. 5B), but it was unable to accumulate ORF44p on the TGN (Fig. 9E).

Downloaded from http://jvi.asm.org/ on December 18, 2013 by KOBE UNIVERSITY

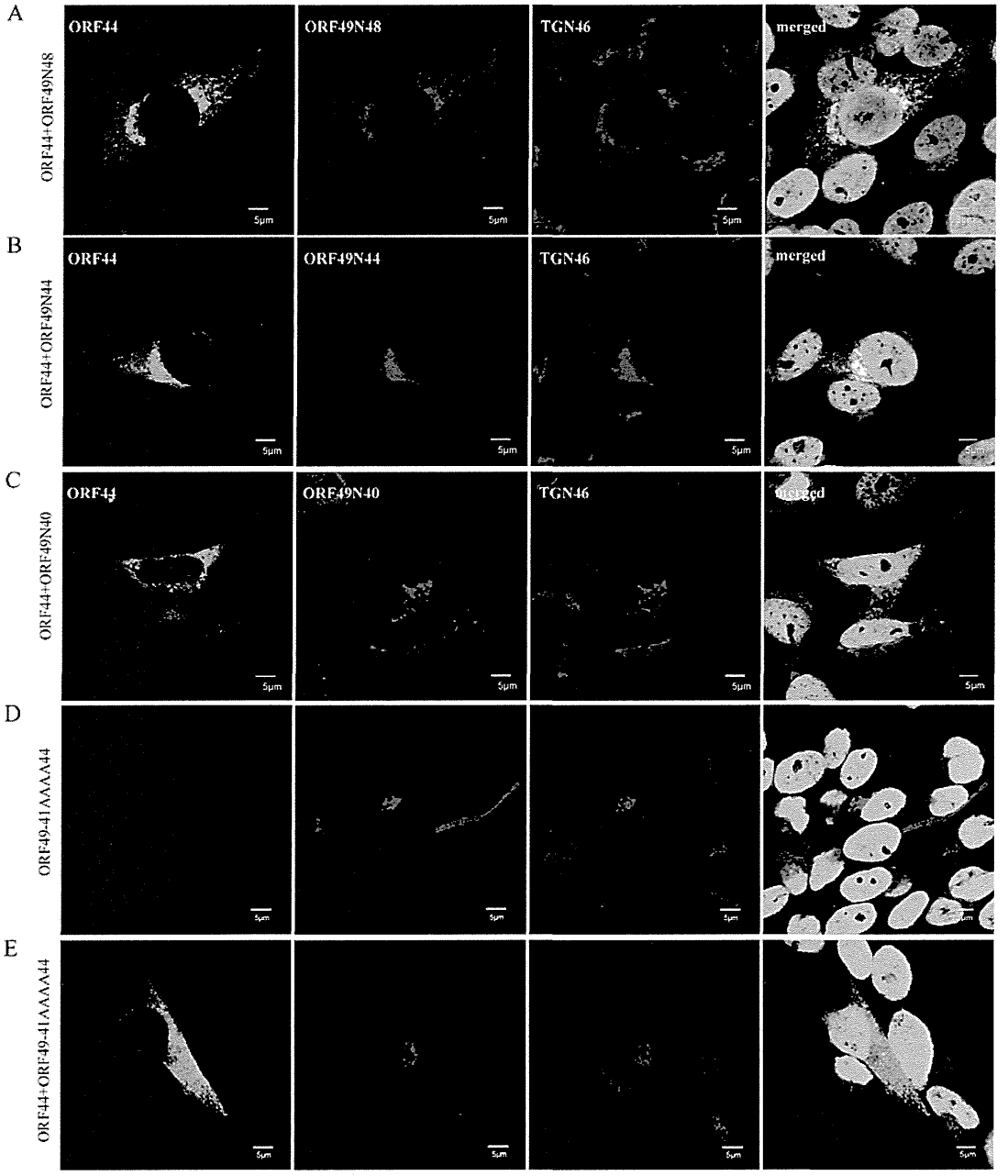


FIG 9 Localization and accumulation of ORF44p in MeWo cells expressing ORF49 mutant proteins. MeWo cells were cotransfected with CAG/ORF44 and CAG/ORF49N48 (A), CAG/ORF49N44 (B), CAG/ORF49N40 (C), or CAG/ORF49-41AAAA44 (E), or transfected with CAG/ORF49-41AAAA44 alone (D). Cells were fixed at 48 h posttransfection and triple labeled for ORF44 (green), ORF49 (red), and TGN46 (blue). Nuclei were stained with Hoechst 33342 (cyan). Scale bars, 5 μm.

Furthermore, ORF49-41AAAA44p did not form a complex with ORF44p or ORF44F129Ap (Fig. 6B, lane 5 or 6) despite the efficient coexpression of all proteins (Fig. 6A, lanes 5 and 6).

The carboxyl-terminal half of the acidic cluster of ORF49p plays a central role in the function of ORF49p during infection. rpOkaORF49-41AAAA44 showed almost the same phenotype as rpOkaORF49M1L, including the loss of the interaction with ORF44p (Fig. 2E, lane 1), the dispersed localization of ORF44p without accumulation on the TGN (Fig. 10A), impaired growth as assessed by plaque size and infectious-center assays (Fig. 11A and B, respectively), and reduced production of infectious progeny virus (to 3 to 10% of the wild-type level [Table 2]), excluding the apparent ORF49-41AAAA44p expression (Fig. 2D, lane 1, and Fig. 10A). These defects were completely rescued by revertant virus infection (Fig. 2D and E, lanes 2, Fig. 10B, and Fig. 11A and B) or by exogenous ORF49p in MeWoORF49 cells (Fig. 11A and B and Table 2). The expression of ORF49-41AAAA44p was detected as a faint and faster-migrating band than that of ORF49p in the revertant virus infection, but an equal amount of ORF44p was detected in both viruses with gH and ORF61p (Fig. 2D, lanes 1 and 2). Furthermore, whereas the interaction between ORF49-41AAAA44p and ORF44p was not detected at all (Fig. 2E, lane 1),

Downloaded from http://jvi.asm.org/ on December 10, 2015 by KOBE UNIVERSITY

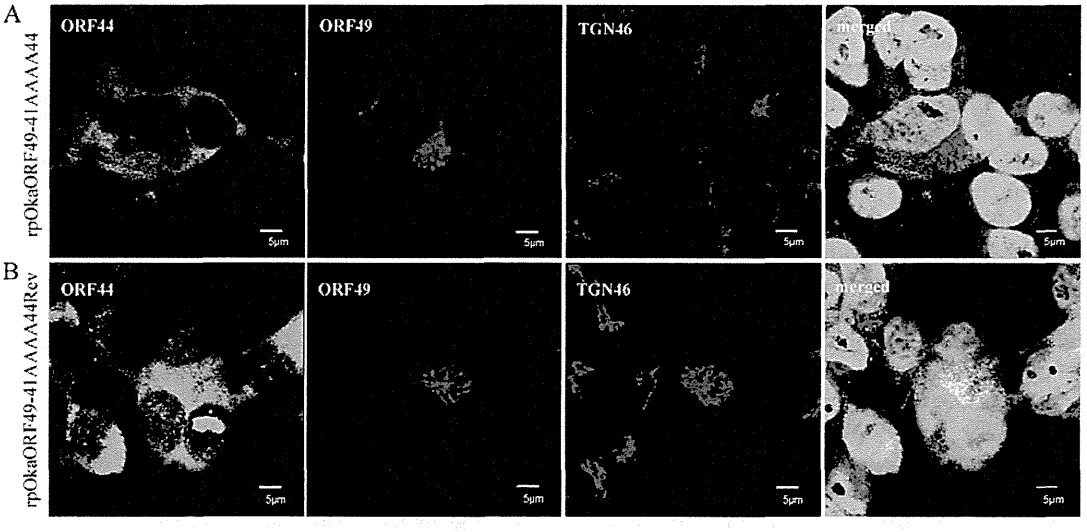


FIG 10 Localization of ORF44p and ORF49p in rpOkaORF49-41AAAA44-infected MeWo cells. rpOkaORF49-41AAAA44-infected MeWo cells (A) and rpOkaORF49-41AAAA44Rev-infected MeWo cells (B) were fixed at 48 hpi and triple labeled for ORF44p (green), ORF49p (red), and TGN46 (blue). Nuclei were stained with Hoechst 33342 (cyan). Scale bars, 5 μm.

ORF44p was incorporated into the rpOkaORF49-41AAAA44 particles in the absence or presence of exogenous ORF49p (Fig. 2F, lane 1 or 2), which was also the case in rpOkaORF49M1L infection (Fig. 2D and F).

Taken together, our results indicated that ORF49p functions in the efficient production of progeny viruses required for VZV infection through its interaction with the essential protein ORF44p.

DISCUSSION

In VZV, ORF49 encodes a nonessential tegument protein that is one of the cell-tropic factors in cell culture (6). In human fetal lung fibroblast MRC-5 cells, the growth of ORF49-defective virus is identical to that of its parental virus, whereas in the human melanoma MeWo cell line, it shows reduced growth; however, the cell tropism of VZV for these two most permissive cell lines has not been studied. In the previous study, we showed that it is a cell-tropic factor, although the step(s) at which ORF49 functions, including the entry, host gene modulation, viral gene expression, viral particle assembly, or egress, remained unclear. Nevertheless, we showed that it may play an important role in the production of a complete virion (6).

VZV is highly cell associated *in vitro*, producing extremely small amounts of infectious virus even when isolated intracellularly (in a particle-to-PFU ratio that varies from approximately 40,000 to 1,000,000) (39, 40), and the particles detected by electron microscopy (EM) analysis appear to be degraded, even in cells infected by the wild-type virus (41–43). The low infectivity and the presence of few or no infectious particles in the cell culture

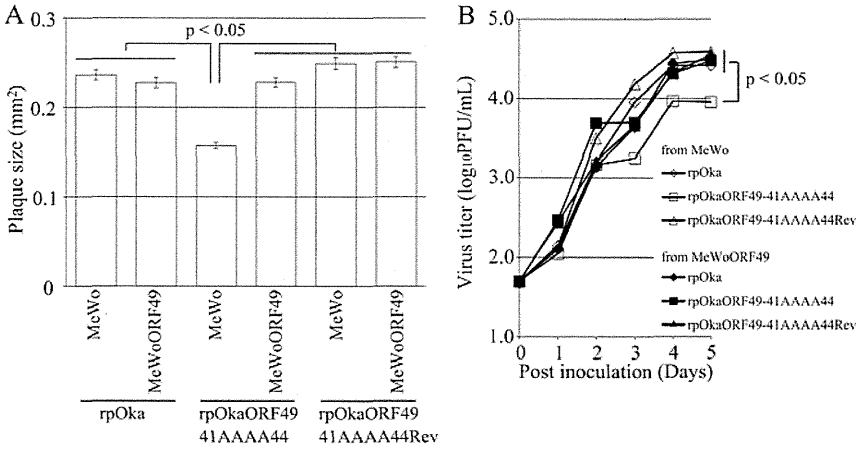


FIG 11 Growth properties of ORF49-41AAAA44 mutant virus in MeWo and MeWoORF49 cells. (A) Comparison of plaque sizes among recombinant viruses. MeWo cells or MeWoORF49 cells were infected with rpOka, rpOkaORF49-41AAAA44, or rpOkaORF49-41AAAA44Rev (50 PFU/well) and cultured for 7 days. Infected cells were stained with an anti-gE Ab, and the plaques were traced and measured by ImageJ software. Plaque size is shown with the standard error of the mean. Statistical significance was determined by Student's *t* test. (B) Growth kinetics of recombinant viruses on MeWo cells and MeWoORF49 cells. MeWo cells or MeWoORF49 cells were infected with rpOka, rpOkaORF49-41AAAA44, or rpOkaORF49-41AAAA44Rev (50 PFU/well), harvested at the indicated times, serially diluted, added to newly prepared MeWo cells, and cultured for 5 days. The plaques were stained with an anti-gE Ab and counted. Each point represents the mean titer for two wells of one experiment. Two experiments were performed independently. Statistical significance was determined by Student's *t* test.

Downloaded from http://jvi.asm.org/ on December 18, 2013 by KOBE UNIVERSITY

supernatant in VZV have made it difficult to construct a *trans*-complementation system. In such a system, the target viral gene is expressed on permissive cells on which the target gene-deleted virus is only capable of efficient replication similar to the wild-type virus infection on the parental cells. The infection of parental cells by the target gene-deleted virus isolated from cells expressing the target gene enables analysis of its function. This method is useful to confirm that the deletion phenotype is not caused by undesired mutations, which can also be determined by generating the revertant virus to repair the mutated gene within the viral genome. In addition, it can also be used to identify the target gene function, which cannot be determined by simply generating the mutant and revertant viruses and has been used widely in the mutagenic analysis of other herpesviruses, especially in the analysis of structural proteins. However, to the best of our knowledge, this system has been used successfully to analyze gene function in only one report (44) and to confirm that the deletion phenotype is independent of undesired mutation in two reports (45, 46) in VZV research.

In the present study, we established a *trans*-complementation system for ORF49. The ORF49 *trans*-complementation system allowed identification of the precise function of ORF49, which could not be determined by generating its defective virus following EM analysis on MeWo cells. In the EM analysis, no significant differences between the wild-type and ORF49-defective viruses were detected with regard to the intracellular and cell surface viral particle counts or morphology (T. Sadaoka and Y. Mori, unpublished observation), possibly leading to their obvious difference in infectivity, which was reduced by 10-fold or higher in the defective virus. Additionally, in both viruses, the infected cells or viral particles isolated from the same quantity of infected cells contained almost the same amount of viral proteins. The *trans*-complementation system in combination with the results of other analyses described above indicated that ORF49 functions in the production of efficient infectious viruses. The results of EM analysis and immunoblotting suggested that the ORF49 defect did not cause the reduction of viral protein synthesis and viral particle assembly and egress. The cell-free virus titration and plaque formation analyses using the *trans*-complementation system showed that the ORF49p released from the virion into the cells during the entry step was not functional, but *de novo* ORF49p synthesized during lytic replication functioned in the production of efficient infectious virus required for cell-free and cell-to-cell viral transmission modes. However, how the deletion of ORF49 impaired infectivity remained unclear.

To gain further insight into the function of ORF49 during VZV infection, we confirmed ORF44p as its binding partner, as reported in other herpesviruses (12–15), and examined the conserved interaction between these proteins by analyzing their binding properties. We identified 129F in ORF44p as being essential for accumulation on the TGN through the interaction with ORF49p: whether it functions in the binding directly or indirectly is unknown. Simultaneously, 41DFDE44 of the carboxyl-terminal half of the acidic cluster within ORF49p was identified as the binding motif for ORF44p. Among these critical amino acids of ORF44p and ORF49p, each phenylalanine seems to function in the binding. As the phenylalanine is an aromatic and hydrophobic amino acid, it prefers to be buried in protein hydrophobic cores. However, 129F of ORF44p is surrounded by polar amino acid 128T and charged amino acid 130K and 42F of ORF49p by charged amino acids 41D, 43D, and 44E, and there is possibility that these two phenylalanines are exposed at the protein surface. The phenylalanine side chain is fairly nonreactive and is thus rarely directly involved in protein function, although it can play a role in substrate recognition. In particular, hydrophobic amino acids can be involved in binding/recognition of hydrophobic ligands, and the aromatic side chain can also be involved in interactions with other aromatic side chains via stacking interactions (47). In coexpression of ORF44 and ORF49, ORF49F42A mutation alone disrupted the interaction and failed to accumulate ORF44p on the TGN, as seen in ORF49-41AAAA44 mutation, while individual ORF49D41A, -D43A, or -E44A mutation had no effect on them (T. Sadaoka and Y. Mori, unpublished observation). On the other hand, ORF44F129A showed an impaired phenotype in terms of their interaction and its accumulation on the TGN, and neither ORF44T128A nor K130A mutation had any effect on them. However, in the context of infection, ORF49F42A alone could not abrogate the interaction and had no effect on virus growth (T. Sadaoka and Y. Mori, unpublished observation) different from that of ORF49-41AAAA44 mutation (discussed below), while only ORF44F129A was truly lethal for infectious virus production/reconstitution, and again ORF44T128A and ORF44K130A had no effect. These findings may prompt us to conclude that the core machinery of the binding is the noncovalent attractive force between two aromatic rings of phenylalanine and that the additional binding force via charged amino acids around 42F of ORF49p is required in the context of infection; however, there is another possibility—that the ORF44F129A mutation just disrupts the protein structure itself, leading to the loss of interaction. As mentioned above, phenylalanine prefers to be buried in protein hydrophobic cores, and the interaction among the aromatic residues is also important in the protein folding and the structural stabilization of protein (48, 49). Our results about the interaction property revealed that the binding domain within ORF44p is located at the first 136 residues and 129F is essentially involved in the binding, but could not be determined as the precise binding domain, and at the same time, there was no apparent degradation or lower expression of ORF44F129Ap in comparison with ORF44p in both prokaryotic expression and eukaryotic expression systems. To address these issues, further analyses by making an N-terminal truncation for refining the interaction domain and another 129F substitution with tyrosine, which differs only in that it contains a hydroxyl group in place of the ortho hydrogen on the benzene ring, for more preferable substitution to maintain structural stability will be helpful and ongoing.

Assessment of the function of ORF44 in the context of infection did not reveal new findings, with the exception of the F129A mutant, which showed the same phenotype as the deletion mutant. The ORF44 deletion and F129A mutation were lethal for progeny virus production/reconstitution in MeWo and MRC-5 cells; however, an effective *trans*-complementation system for ORF44 as for ORF49 was not successfully established, and at what step(s) in the lytic infection ORF44 essentially functions remained unclear. To find the nonessential but important functions of ORF44 in the context of infection, we turned back to analyzing the ORF49 function by generating ORF49-41AAAA44 virus, in which ORF49p specifically lost the interaction with ORF44p, following comparison of the phenotype between ORF49-defective virus and ORF49-41AAAA44 virus. The rpOkaORF49-41AAAA44 virus showed the same phenotype as the rpOkaORF49M1L virus, indicating that the function of ORF49p in the efficient production of

Downloaded from http://jvi.asm.org/ on December 10, 2015 by KYOTO UNIVERSITY

progeny viruses was completely dependent on the interaction with ORF44p at 41DFDE44. These results suggest that ORF44p is fully functional only in the presence of ORF49p and vice versa and has essential functions during infection, which are independent of the interaction with ORF49p or redundantly supported by other viral factors in the absence of ORF49p.

In the absence of the interaction with ORF49p during infection, ORF44p was detected throughout the cytoplasm and rarely colocalized with the TGN (or with a reorganized organ containing TGN-derived membranes known to be induced by viral infection, although it has not been found in VZV infection), the recognized site of viral assembly; however, incorporation of ORF44p into viral particles was comparable to that observed in wild-type virus infection. These results indicate that ORF44p was not directly incorporated into the particles through the TGN via its interaction with ORF49p, at least in the absence of ORF49p. In HSV-1, the amount of pUL16 packaged into the viral particles was severely reduced in the absence of pUL11 (50), but there are some other interaction partners that potentially function in incorporating pUL16 into the viral particles (i.e., pUL21 and glycoprotein E) (51, 52). In VZV, by global screening using the yeast two-hybrid system, some candidates for ORF44p binding partner have been reported (28, 29), but in our observations, none of these viral proteins other than ORF49p could accumulate ORF44p on the TGN; one viral protein could alter the localization of ORF44p into the nucleus; however, whether it functions in the incorporation of ORF44p into the viral particles remained unclear (T. Sadaoka and Y. Mori, unpublished observation). Anyway, additional ORF44p binding partners active during either the wild-type virus or ORF49-defective virus infection remain to be identified so far, and the complexity of the herpesvirus protein-protein network requires a solid approach to elucidate the essential roles of ORF44 during viral infection further through the interactions with other viral proteins.

In summary, in the present study, we established a *trans*-complementation system for ORF49 and identified ORF44p as the binding partner for ORF49p. We showed that (i) ORF49p functions in the efficient production of infectious virus, (ii) no other viral factor is required for binding, (iii) residue 129F of ORF44p is critical not only for binding to ORF49p but also for progeny virus production/reconstitution, (iv) the carboxyl-terminal half of the acidic cluster (41DFDE44) of ORF49p is the binding motif for ORF44p, and (v) the efficient production of infectious progeny virus by ORF49p is dependent on its interaction with ORF44p. Further analyses of the role of ORF44 mediated by its interaction with ORF49 or other as yet unidentified viral proteins may shed light on the conserved infection mechanisms of the *Herpesvirinae* and those unique to VZV.

ACKNOWLEDGMENTS

We thank Eiko Moriishi (National Institute of Biomedical Innovation, Osaka, Japan) for technical assistance, Panayiotis A. Ioannou (Cell and Gene Therapy Research Group, The Murdoch Children's Research Institute, The University of Melbourne, Royal Children's Hospital, Melbourne, Australia) for providing pGETrec, Wilfried Wackernagel (Genetics, Department of Biology and Environmental Sciences, Universität Oldenburg, Germany) for pCP20, Jun-ichi Miyazaki (Division of Stem Cell Regulation Research, Osaka University Graduate School of Medicine, Japan) for pCAGGS, Masaru Okabe (Department of Experimental Genome Research, Genome Information Research Center, Osaka University, Japan) for pCX-Cre, and Ulrich H. Koszinowski (Max von Pettenkofer Institut fur Virologie, Ludwig-Maximilians-Universität München, Germany) for pHA2 and pST76A-SR.

This study was supported in part by a Grant-in-Aid for Scientific Research on Priority Areas (21022031 to Y.M.) from the Ministry of Education, Culture, Sports, Science, and Technology (MEXT) of Japan, a Grant-in-Aid for Scientific Research (B) (20390138 to Y.M.), a Grant-in-Aid for Young Scientists (B) (20790363 and 22790432 to T.S.), a Grant-in-Aid for Scientific Research (C) (24590551 to T.S.) from the Japan Society for the Promotion of Science (JSPS), and a grant from the Uehara Memorial Foundation (to T.S.).

REFERENCES

1. **Moffat J, Ku CC, Zerboni L, Sommer M, Arvin A.** 2007. VZV: pathogenesis and the disease consequences of primary infection, p 675–688. *In* Arvin A, Campadelli-Fiume G, Mocarski E, Moore PS, Roizman B, Whitley R, Yamanishi K (ed), Human herpesviruses: biology, therapy, and immunoprophylaxis. Cambridge University Press, Cambridge, United Kingdom.
2. **Baines JD, Pellett PE.** 2007. Genetic comparison of human alphaherpesvirus genomes, p 61–69. *In* Arvin A, Campadelli-Fiume G, Mocarski E, Moore PS, Roizman B, Whitley R, Yamanishi K (ed), Human herpesviruses: biology, therapy, and immunoprophylaxis. Cambridge University Press, Cambridge, United Kingdom.
3. **Davison AJ, Scott JE.** 1986. The complete DNA sequence of varicella-zoster virus. J. Gen. Virol. **67**:1759–1816. http://dx.doi.org/10.1099/0022-1317-67-9-1759.
4. **Davison AJ.** 2007. Comparative analysis of the genomes, p 10–26. *In* Arvin A, Campadelli-Fiume G, Mocarski E, Moore PS, Roizman B, Whitley R, Yamanishi K (ed), Human herpesviruses: biology, therapy, and immunoprophylaxis. Cambridge University Press, Cambridge, United Kingdom.
5. **Zhang Z, Selariu A, Warden C, Huang G, Huang Y, Zaccheus O, Cheng T, Xia N, Zhu H.** 2010. Genome-wide mutagenesis reveals that ORF7 is a novel VZV skin-tropic factor. PLoS Pathog. **6**:e1000971. http://dx.doi.org/10.1371/journal.ppat.1000971.
6. **Sadaoka T, Yoshii H, Imazawa T, Yamanishi K, Mori Y.** 2007. Deletion in open reading frame 49 of varicella-zoster virus reduces virus growth in human malignant melanoma cells but not in human embryonic fibroblasts. J. Virol. **81**:12654–12665. http://dx.doi.org/10.1128/JVI.01183-07.
7. **Baines JD, Jacob RJ, Simmerman L, Roizman B.** 1995. The herpes simplex virus 1 UL11 proteins are associated with cytoplasmic and nuclear membranes and with nuclear bodies of infected cells. J. Virol. **69**:825–833.
8. **Britt WJ, Jarvis M, Seo JY, Drummond D, Nelson J.** 2004. Rapid genetic engineering of human cytomegalovirus by using a lambda phage linear recombination system: demonstration that pp28 (UL99) is essential for production of infectious virus. J. Virol. **78**:539–543. http://dx.doi.org/10.1128/JVI.78.1.539-543.2004.
9. **Silva MC, Yu QC, Enquist L, Shenk T.** 2003. Human cytomegalovirus UL99-encoded pp28 is required for the cytoplasmic envelopment of tegument-associated capsids. J. Virol. **77**:10594–10605. http://dx.doi.org/10.1128/JVI.77.19.10594-10605.2003.
10. **MacLean CA, Dolan A, Jamieson FE, McGeoch DJ.** 1992. The myristylated virion proteins of herpes simplex virus type 1: investigation of their role in the virus life cycle. J. Gen. Virol. **73**:539–547. http://dx.doi.org/10.1099/0022-1317-73-3-539.
11. **Silva MC, Schroer J, Shenk T.** 2005. Human cytomegalovirus cell-to-cell spread in the absence of an essential assembly protein. Proc. Natl. Acad. Sci. U. S. A. **102**:2081–2086. http://dx.doi.org/10.1073/pnas.0409597102.
12. **Loomis JS, Courtney RJ, Wills JW.** 2003. Binding partners for the UL11 tegument protein of herpes simplex virus type 1. J. Virol. **77**:11417–11424. http://dx.doi.org/10.1128/JVI.77.21.11417-11424.2003.
13. **Guo H, Wang L, Peng L, Zhou ZH, Deng H.** 2009. Open reading frame 33 of a gammaherpesvirus encodes a tegument protein essential for virion morphogenesis and egress. J. Virol. **83**:10582–10595. http://dx.doi.org/10.1128/JVI.00497-09.
14. **Liu Y, Cui Z, Zhang Z, Wei H, Zhou Y, Wang M, Zhang XE.** 2009. The tegument protein UL94 of human cytomegalovirus as a binding partner for tegument protein pp28 identified by intracellular imaging. Virology **388**:68–77. http://dx.doi.org/10.1016/j.virol.2009.03.007.
15. **Maninger S, Bosse JB, Lemnitzer F, Pogoda M, Mohr CA, von Einem J, Walther P, Koszinowski UH, Ruzsics Z.** 2011. M94 is essential for the

Downloaded from http://jvi.asm.org/ on December 18, 2013 by KOBE UNIVERSITY